

Watching nanomaterials with X-ray eyes: probing different length scales by combining scattering with spectroscopy

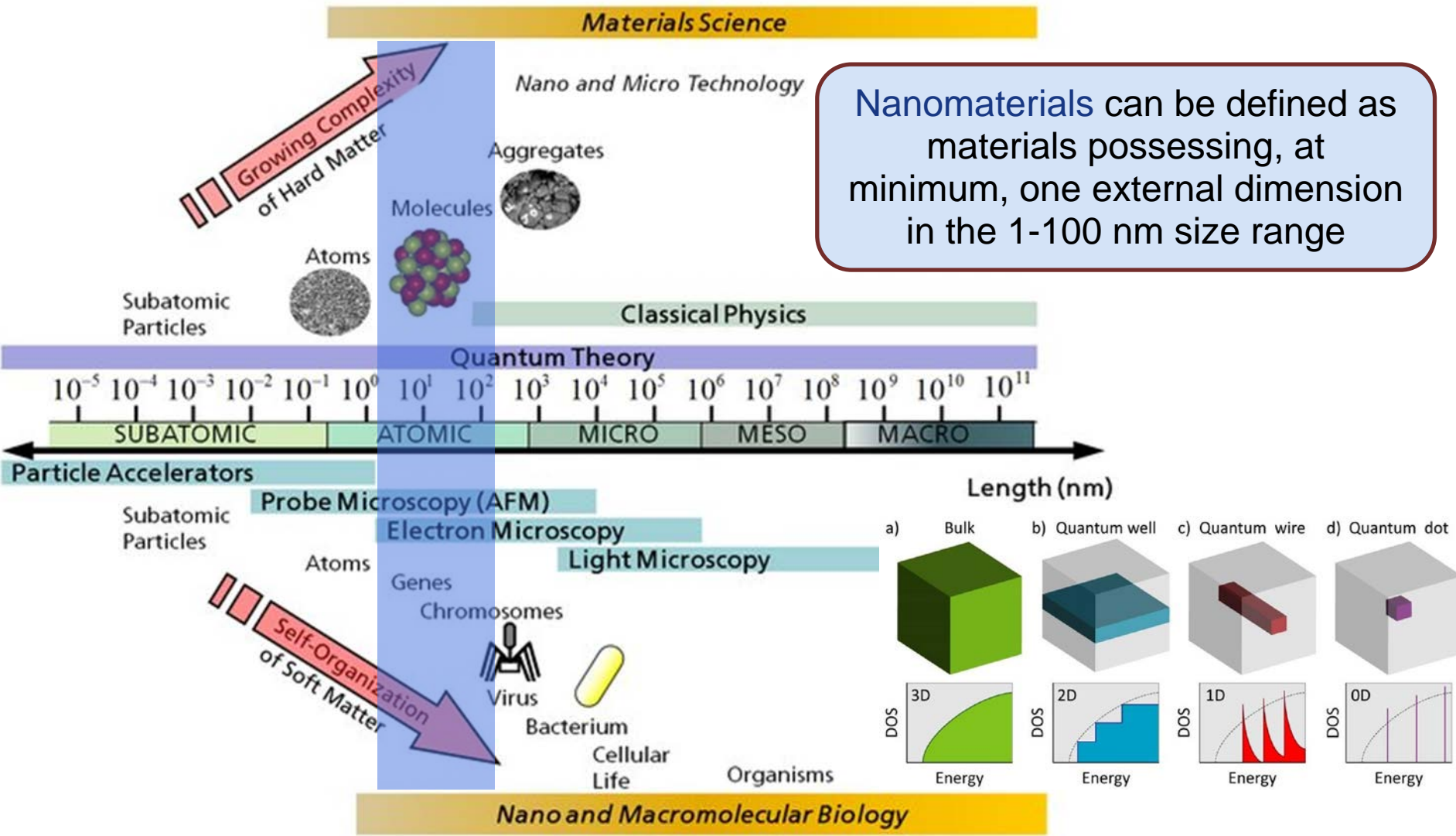
Lorenzo Mino

Department of Chemistry and NIS, University of Torino

School on Synchrotron Radiation "Gilberto Vlaic", 13-17 September 2021

Nanomaterials

Nanomaterials can be defined as materials possessing, at minimum, one external dimension in the 1-100 nm size range



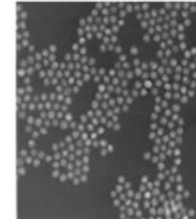
Nanotechnology: unintentional beginning



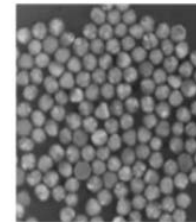
Lycurgus Cup
(4th-century)



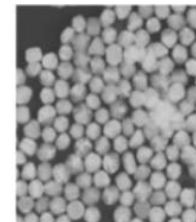
Gold and silver nanoparticles can be used to produce stained glass windows.



Silver - spheres
Size: 40 nm
Reflected color: Dark blue



Silver - spheres
Size: 80 nm
Reflected color: Celestial blue



Silver - spheres
Size: 100 nm
Reflected color: Shiny gold

Medieval stained glass

Nanotechnology: conceptual origins

There's Plenty of Room at the Bottom

29 December 1959, annual meeting of the American Physical Society, California Institute of Technology (Caltech)



Richard Feynman
(Nobel Prize in Physics 1965)

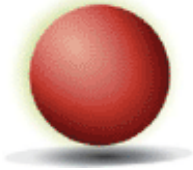


Norio Taniguchi

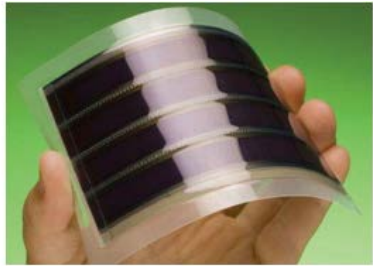
Coined the term «**nano-technology**» in 1974 referring to «ultra precision materials processing technologies»

Nanomaterials applications

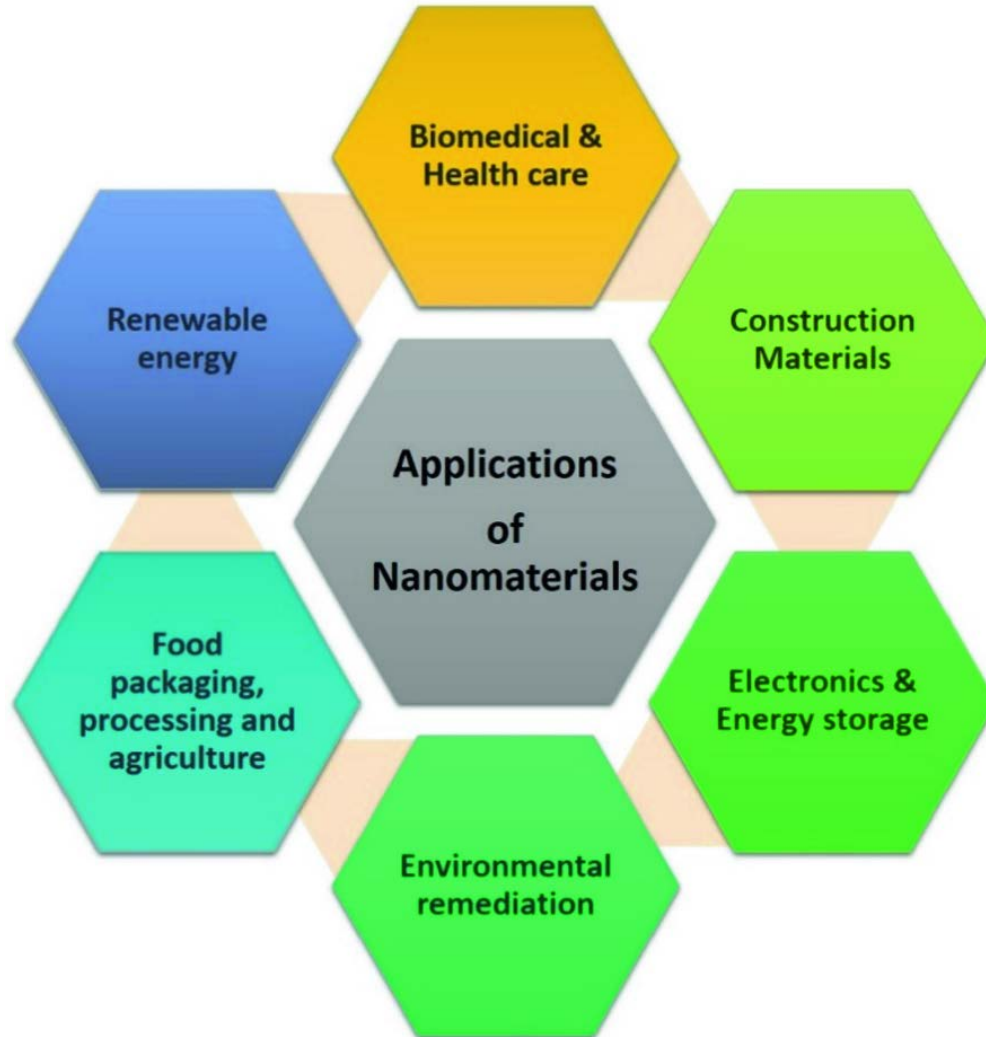
Gold nanoparticle



Mesoporous silica nanoparticle



Carbon nanotube

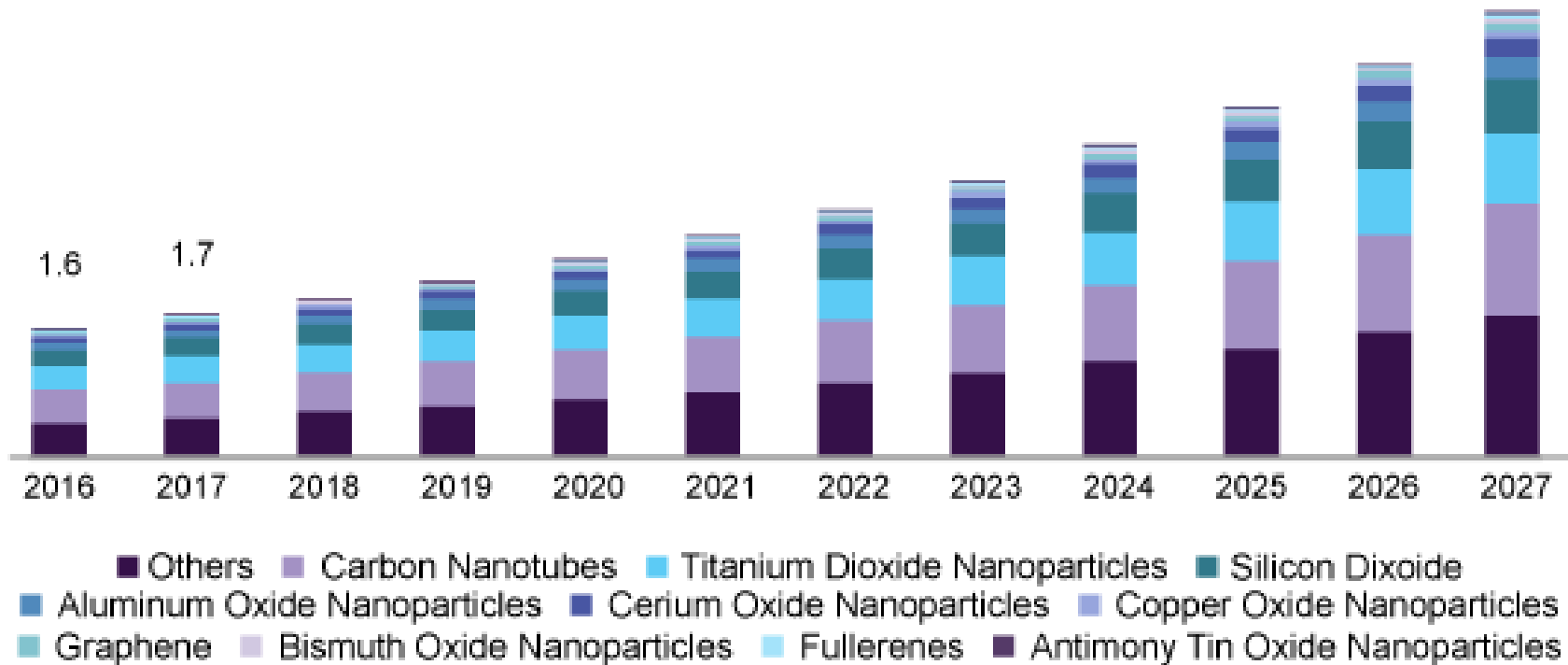


Quantum dot



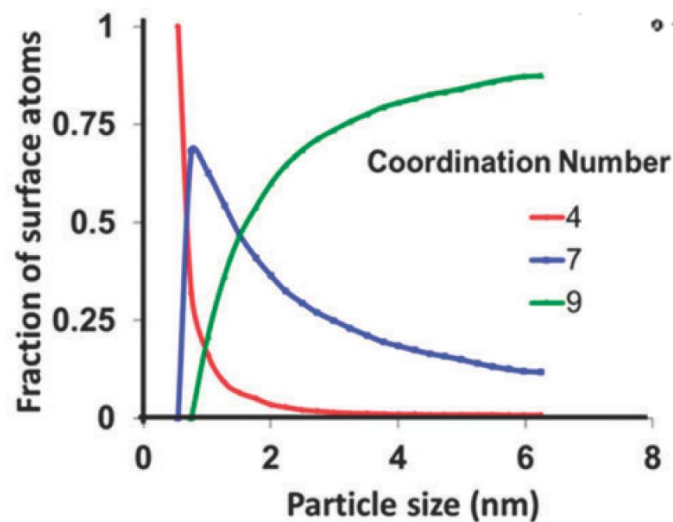
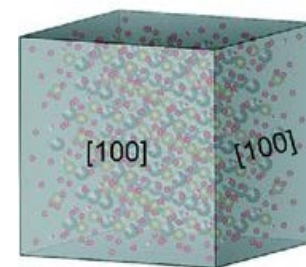
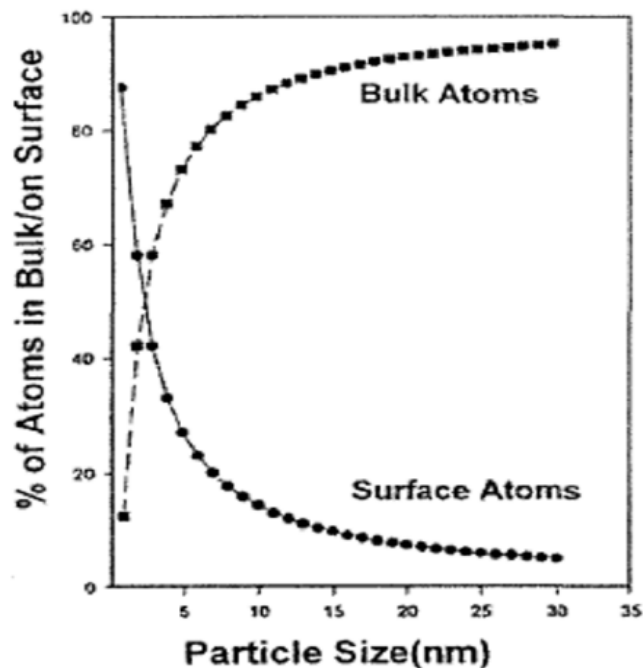
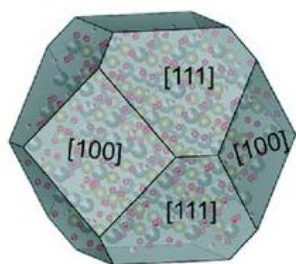
Nanomaterials market

U.S. nanomaterials market size, by product, 2016 - 2027 (USD Billion)

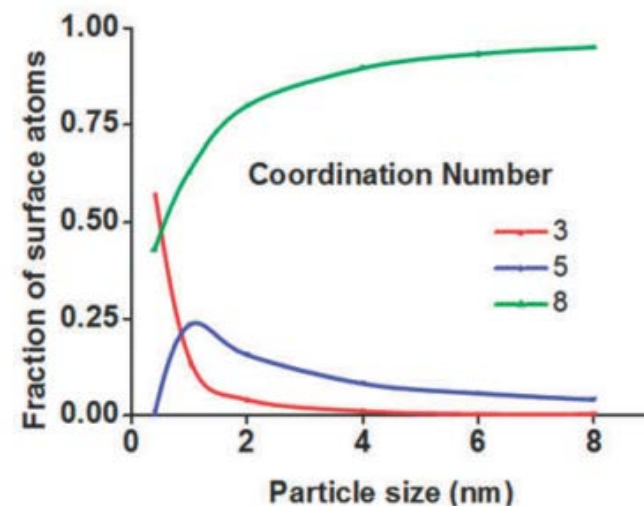


Source: www.grandviewresearch.com

Nanomaterials properties



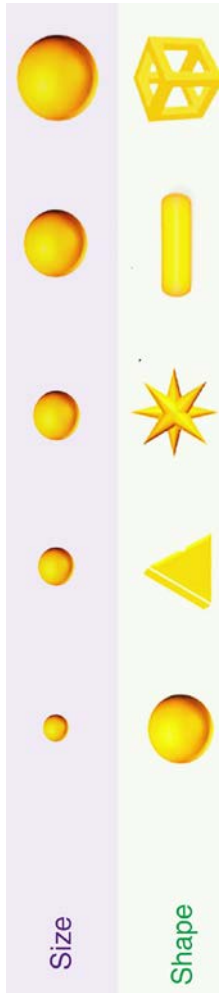
Catalytic activity is strongly shape and size dependent



S.Cao et al., Chem. Soc. Rev., 2016, 45, 4747--4765

Nanomaterials properties

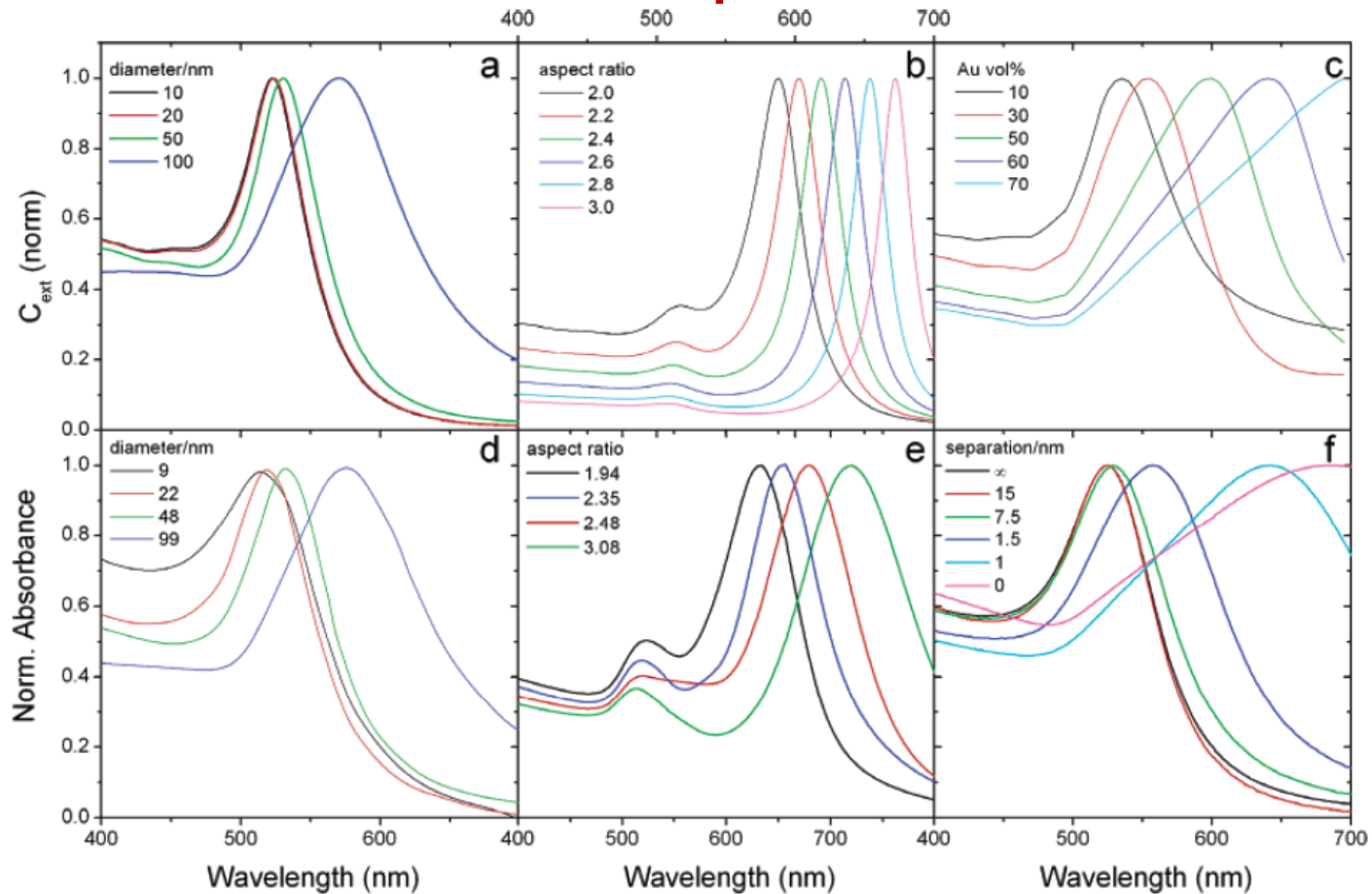
Au NPs optical properties



Size

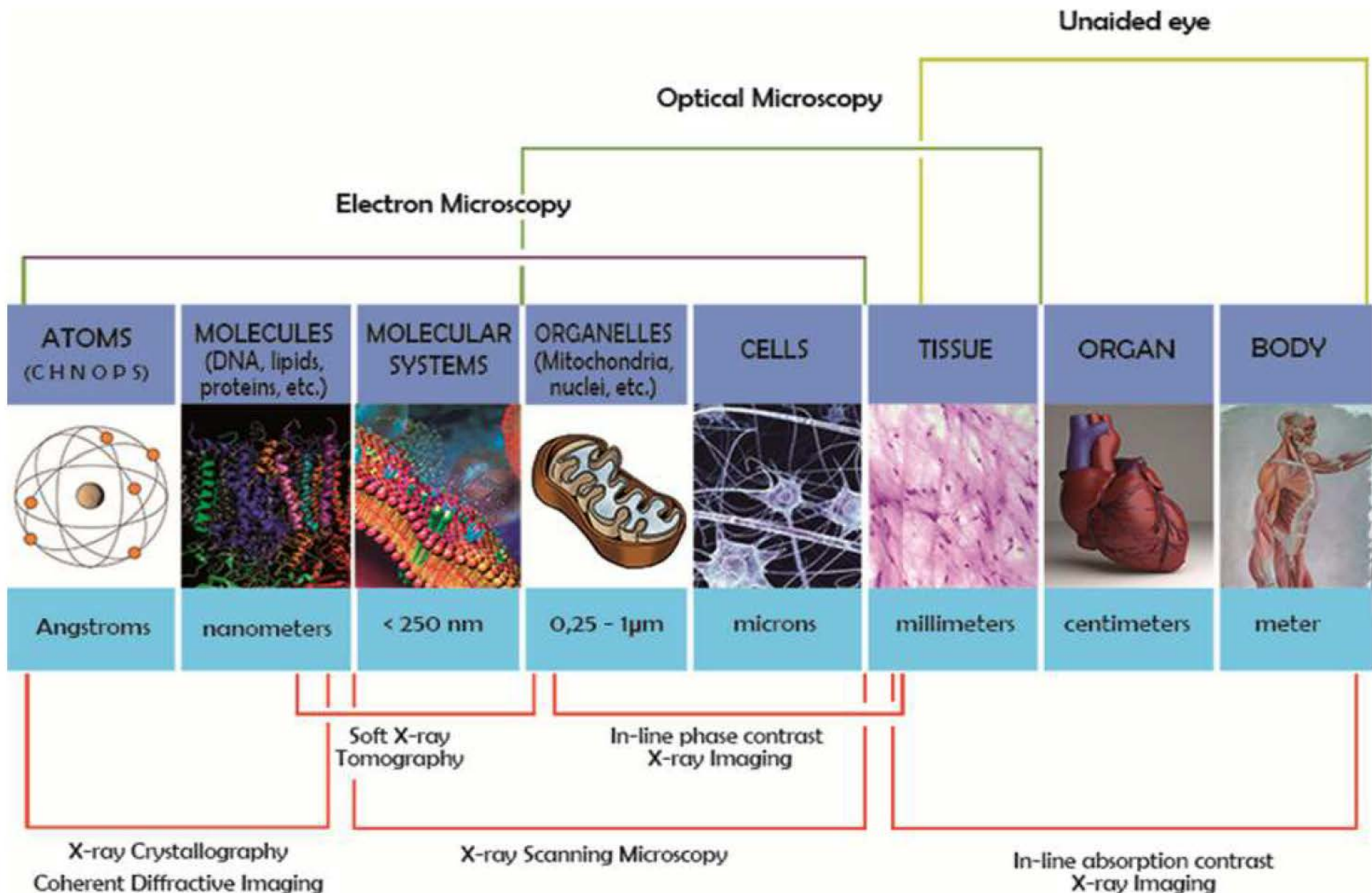
Shape

Interparticle distance



Top: Calculated UV–visible spectra for (a) Au spheres with varying diameters, (b) Au ellipsoids of varying aspect ratio, and (c) thin glass films loaded with increasing Au nanoparticle volume fractions. Bottom: Experimental spectra for (d) Au spheres,⁴⁰ (e) Au nanorods, and (f) multilayer films of glass-coated Au spheres with varying interparticle distance.

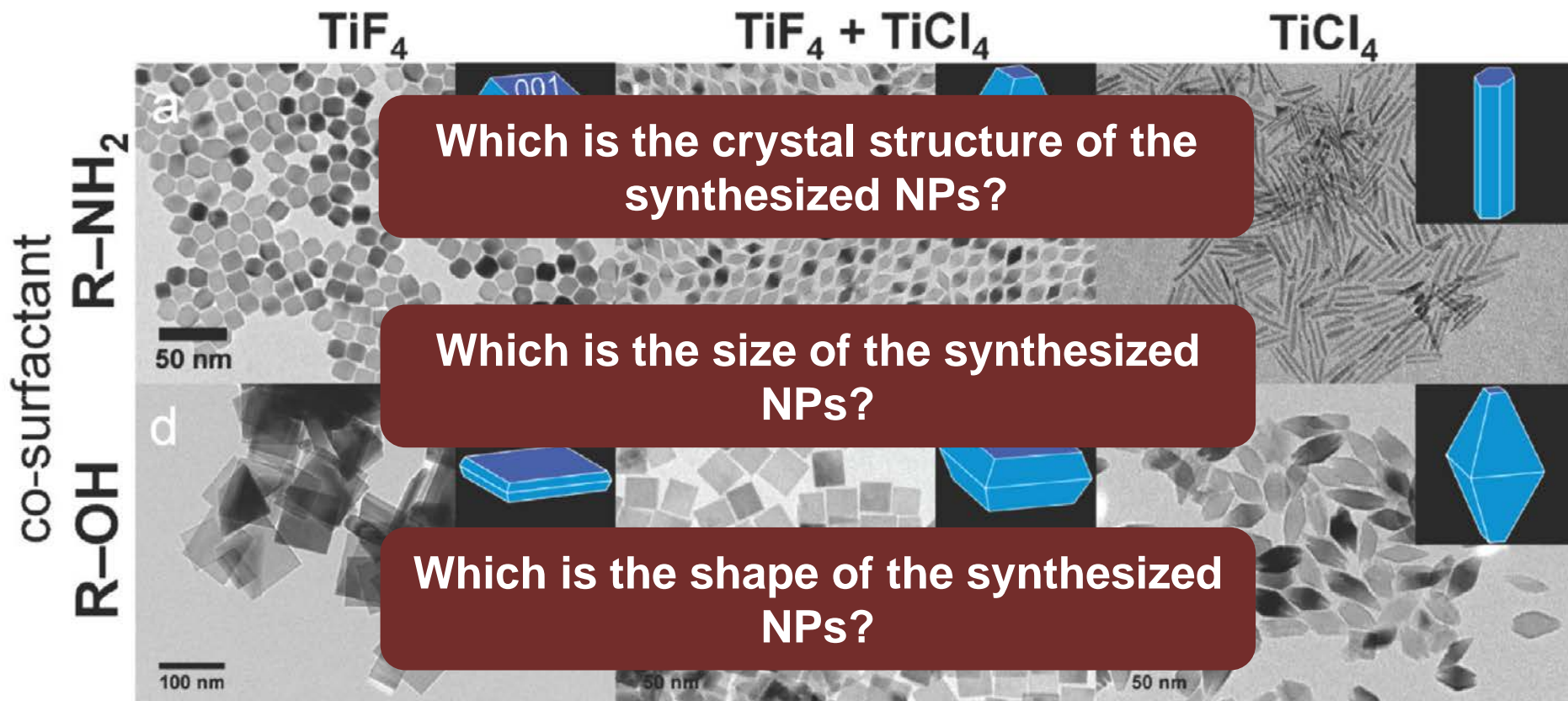
Probing different length scales



**Let's start with a
simple case:
nanoparticles...**

X-ray techniques in nanoparticles characterization

TiO₂ nanoparticles

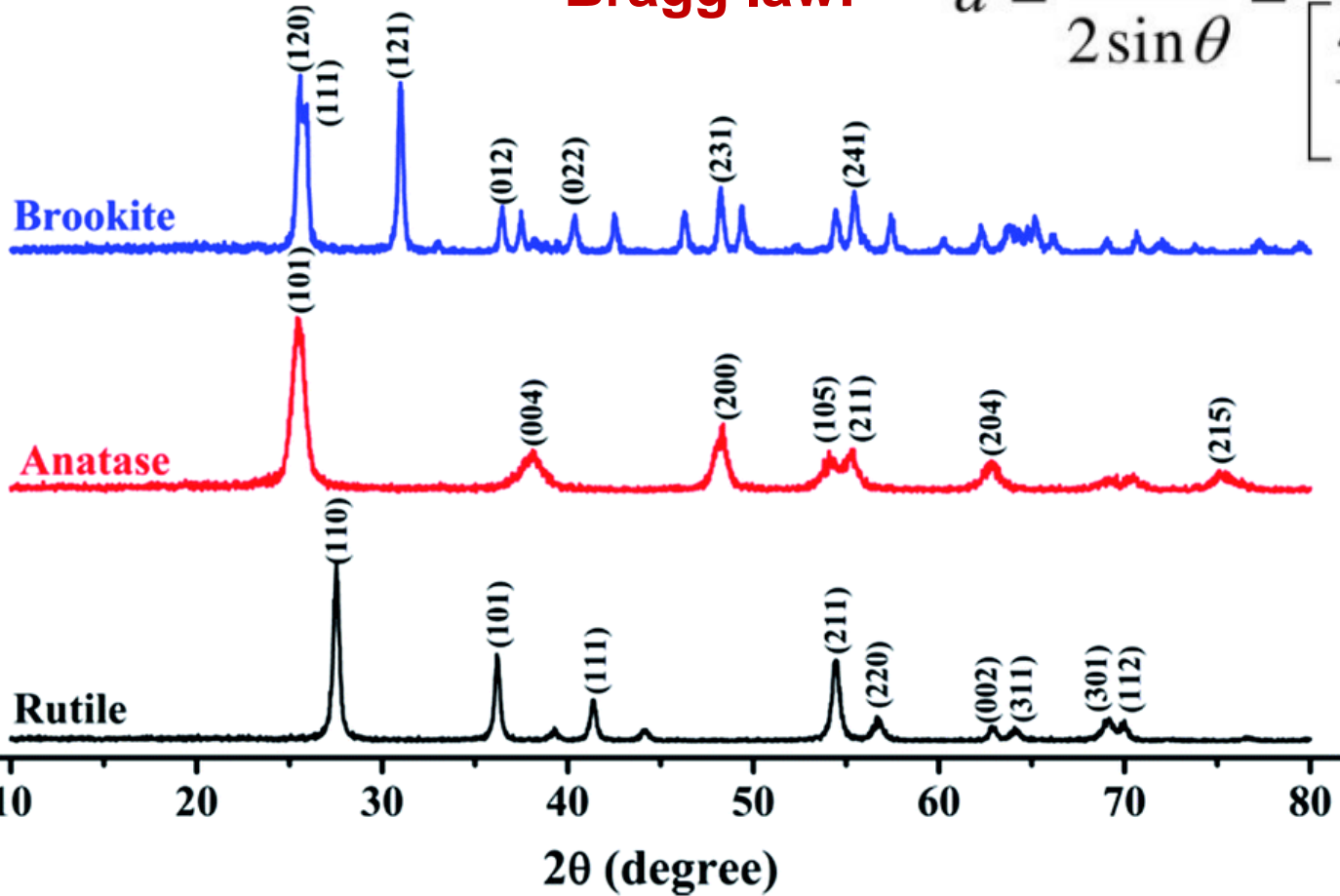


T.. Gordon et al., J. Am. Chem. Soc. 2012, 134, 6751 – 6761

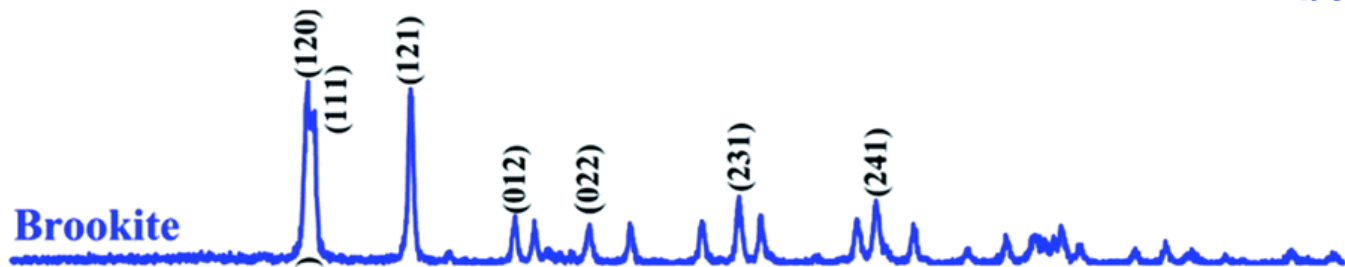
Which is the NPs crystal structure?

Bragg law:

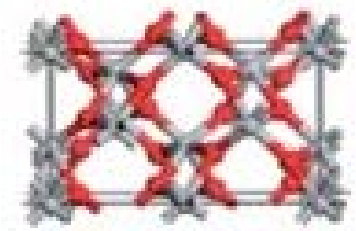
$$d = \frac{\lambda}{2 \sin \theta} = \left[\frac{4\pi}{\lambda} \right] \sin \theta = \frac{2\pi}{q}$$



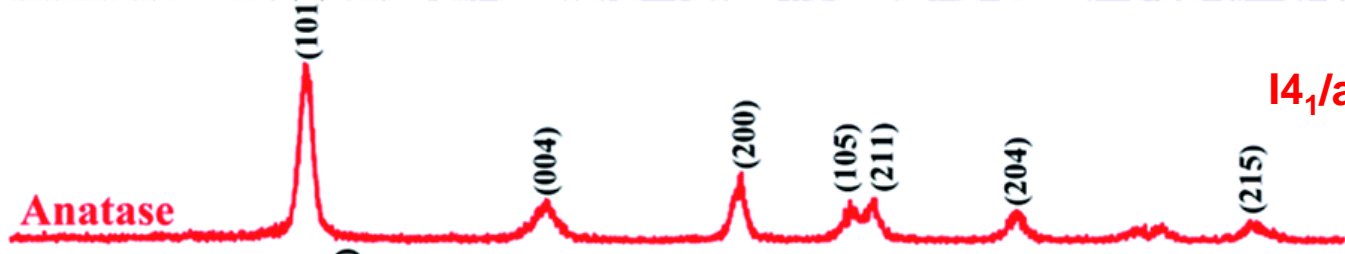
Which is the NPs crystal structure?



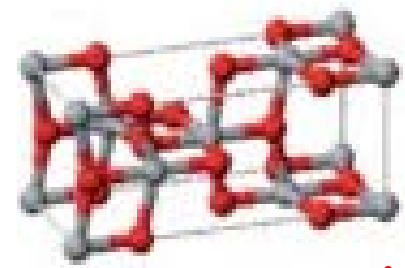
Pbca



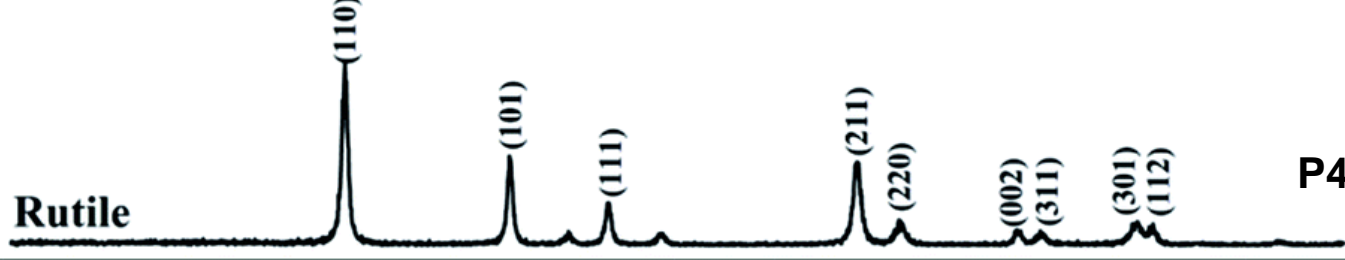
$a = 5.455 \text{ \AA}$
 $b = 9.181 \text{ \AA}$
 $c = 5.142 \text{ \AA}$



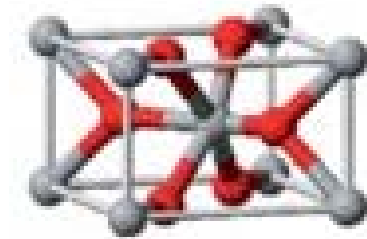
$I4_1/amd$



$a = b = 3.785 \text{ \AA}$
 $c = 9.512 \text{ \AA}$



$P4_2/mnm$

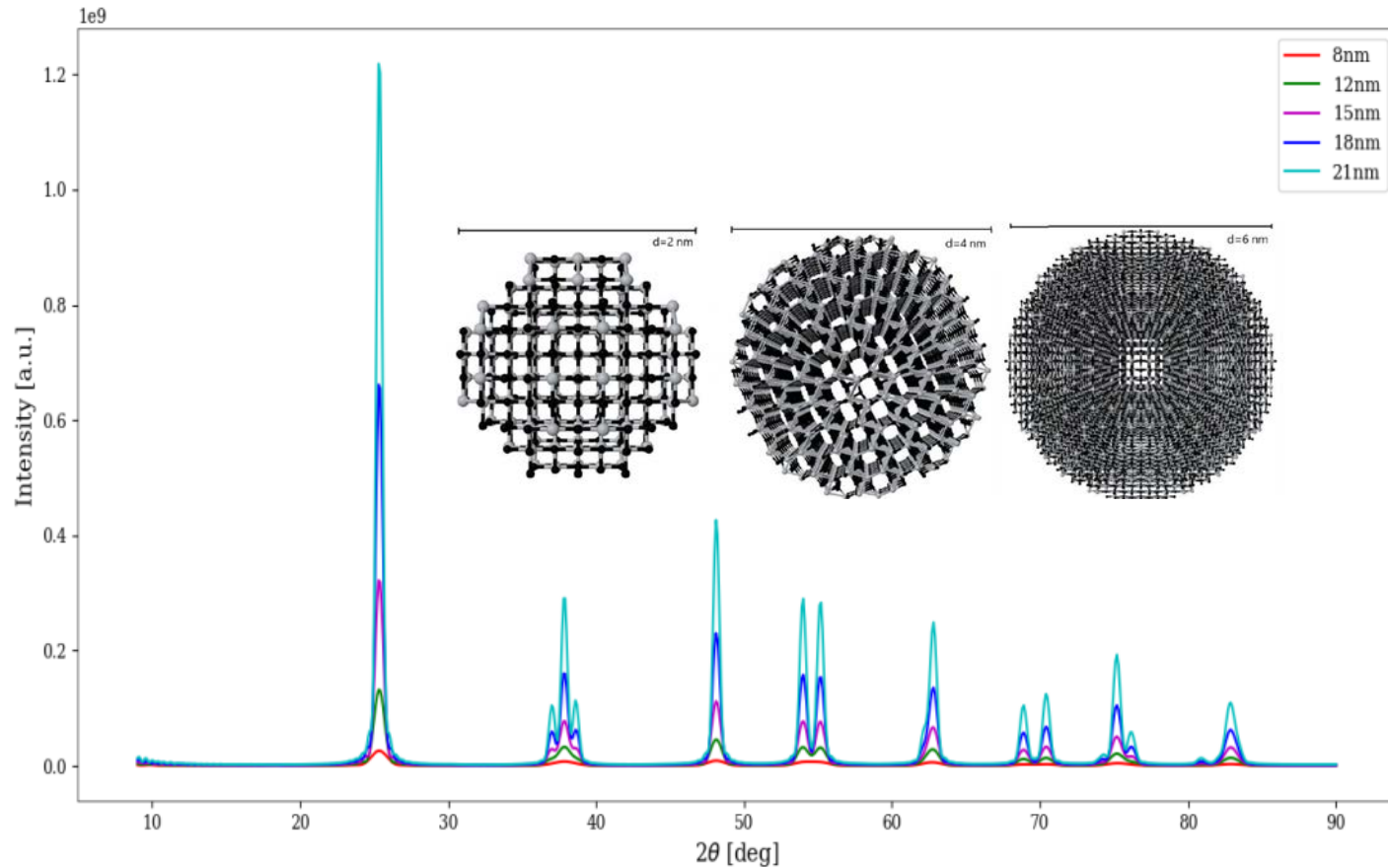


$a = b = 4.593 \text{ \AA}$
 $c = 2.959 \text{ \AA}$

10 20 30 40 50 60 70 80

2θ (degree)

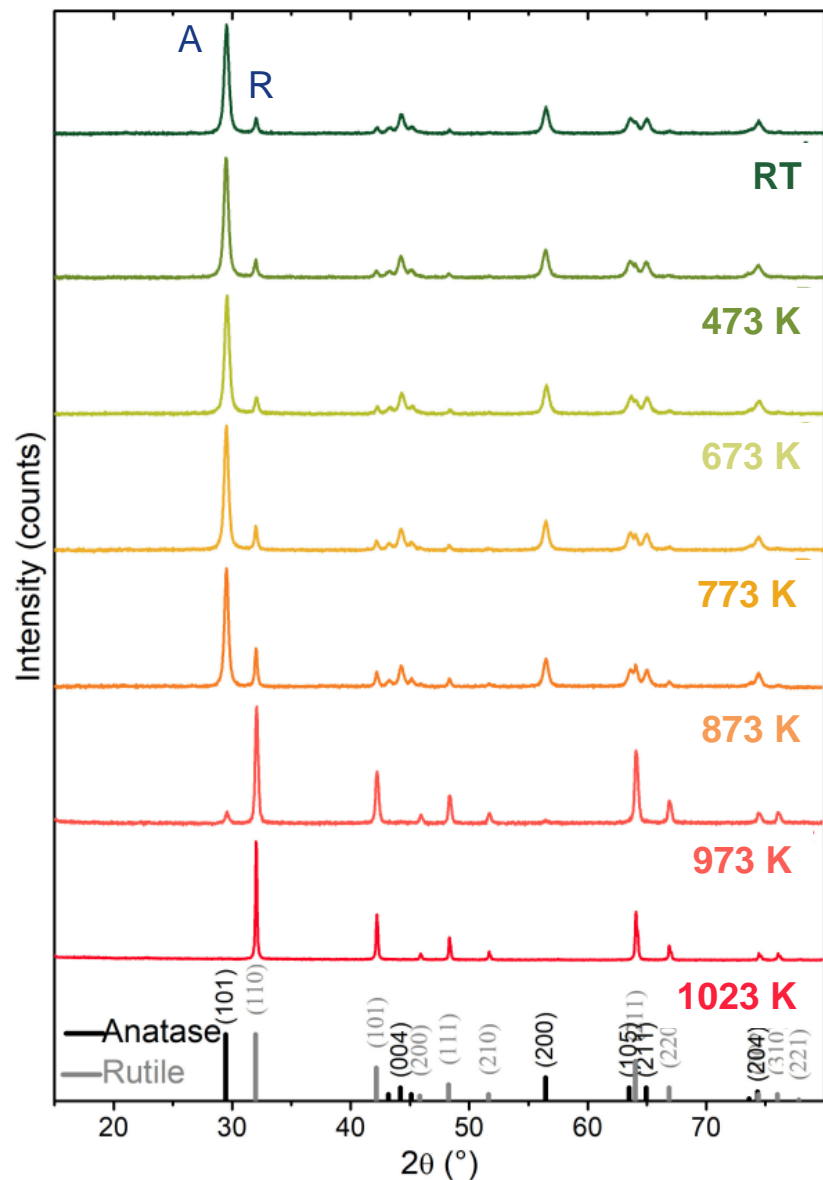
Which is the NPs size?



Scherrer equation:

$$L = \frac{K\lambda}{(\beta_{\text{exp}} - \beta_{\text{strum}}) \cos \theta}$$

Monitoring NP sintering and phase transitions

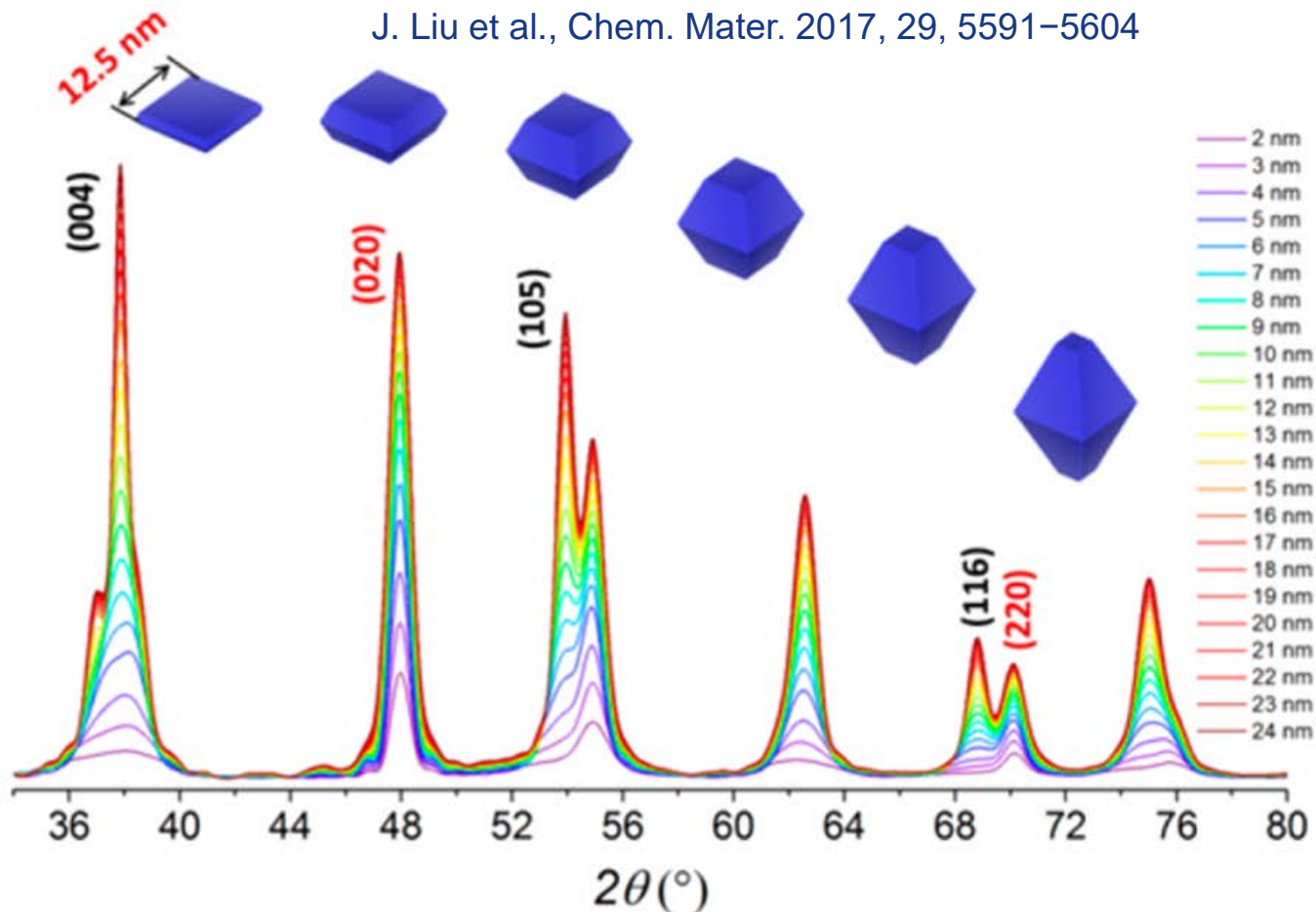


Temperature of treatments ^a	Phase composition ^b		Crystallite sizes ^c	
	Anatase (wt%)	Rutile (wt%)	Anatase (nm)	Rutile (nm)
RT	83	17	28	47
473 K	83	17	28	47
673 K	83	17	28	47
773 K	80	20	33	56
873 K	59	41	35	60
973 K	7	93	48	62
1,023 K		100		237

M. J. Uddin et al., Front. Mater. 2020, 7, 192.

Which is the NPs shape?

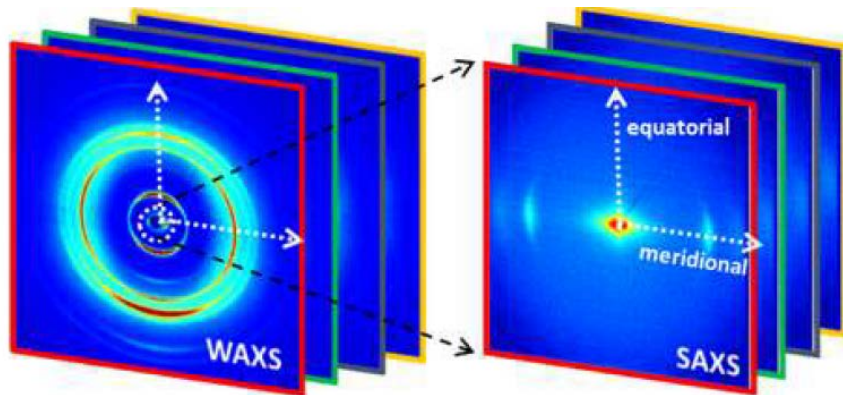
J. Liu et al., Chem. Mater. 2017, 29, 5591–5604



The relative intensity and FWHM of the XRD peaks depends on the NPs shape

Small angle X-ray scattering (SAXS)


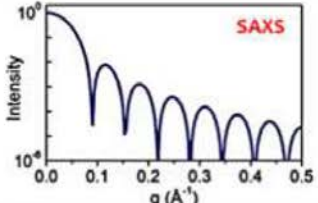
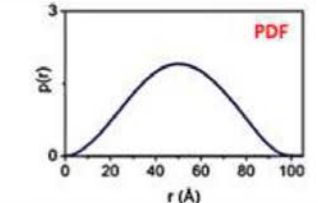

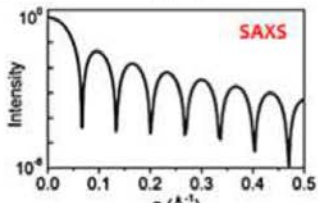
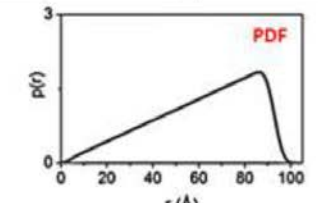
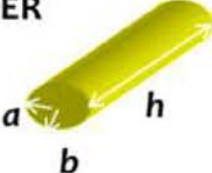
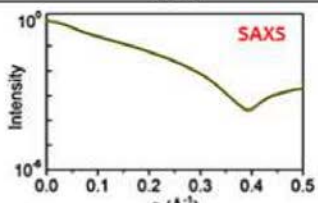
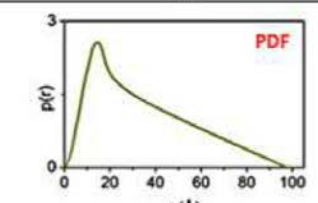

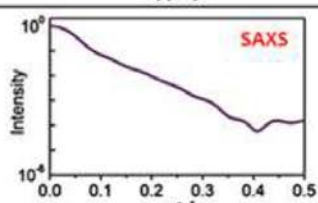
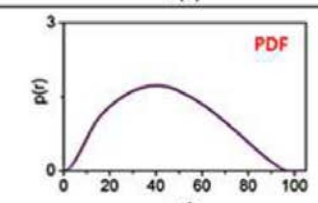
Technique	d (nm)	q (nm ⁻¹)	q (Å ⁻¹)	θ(deg) for λ=1.5405Å
SAXS/SAXD	100	0.063	0.0063	0.044
SAXS/SAXD	10	0.63	0.063	0.44
WAXS/WAXD	1	6.3	0.63	4.4
WAXS/WAXD	0.1	63	6.3	50.6



$$d = \frac{\lambda}{2 \sin \theta} = \frac{2\pi}{\left[\frac{4\pi}{\lambda} \right] \sin \theta} = \frac{2\pi}{q}$$

C. Giannini et al., Prog. Mater. Sci. 2020, 112, 100667

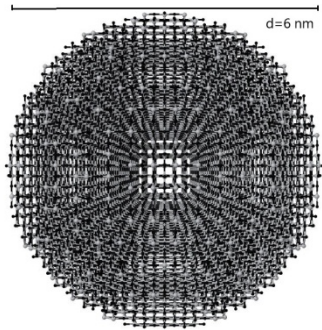
SAXS: shape and size

<p>SPHERE</p> 			$R_g^2 = \frac{3}{5} R^2$
<p>HOLLOW SPHERE</p> 			$R_g^2 = \frac{3 R_2^5 - R_1^5}{5 R_2^3 - R_1^3}$
<p>CYLINDER</p> 			$R_g^2 = \frac{a^2 + b^2}{4} + \frac{h^2}{12}$
<p>FLAT DISK</p> 			$R_g^2 = \frac{R^2}{2} + \frac{h^2}{12}$

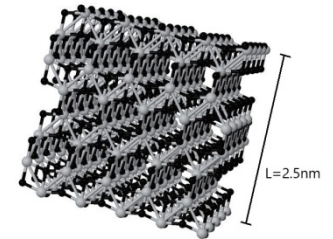
The gyration radius (R_g) can be linked to the main dimensions of the object

C. Giannini et al., Prog. Mater. Sci. 2020, 112, 100667

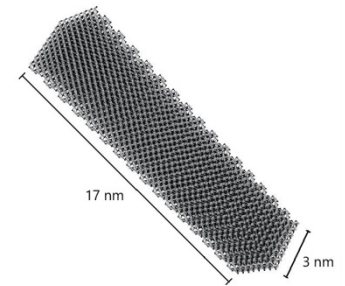
The Debye scattering equation



$$I(q) = I_0 \sum_m \sum_n F_m F_n \frac{\sin(qr_{mn})}{qr_{mn}}$$

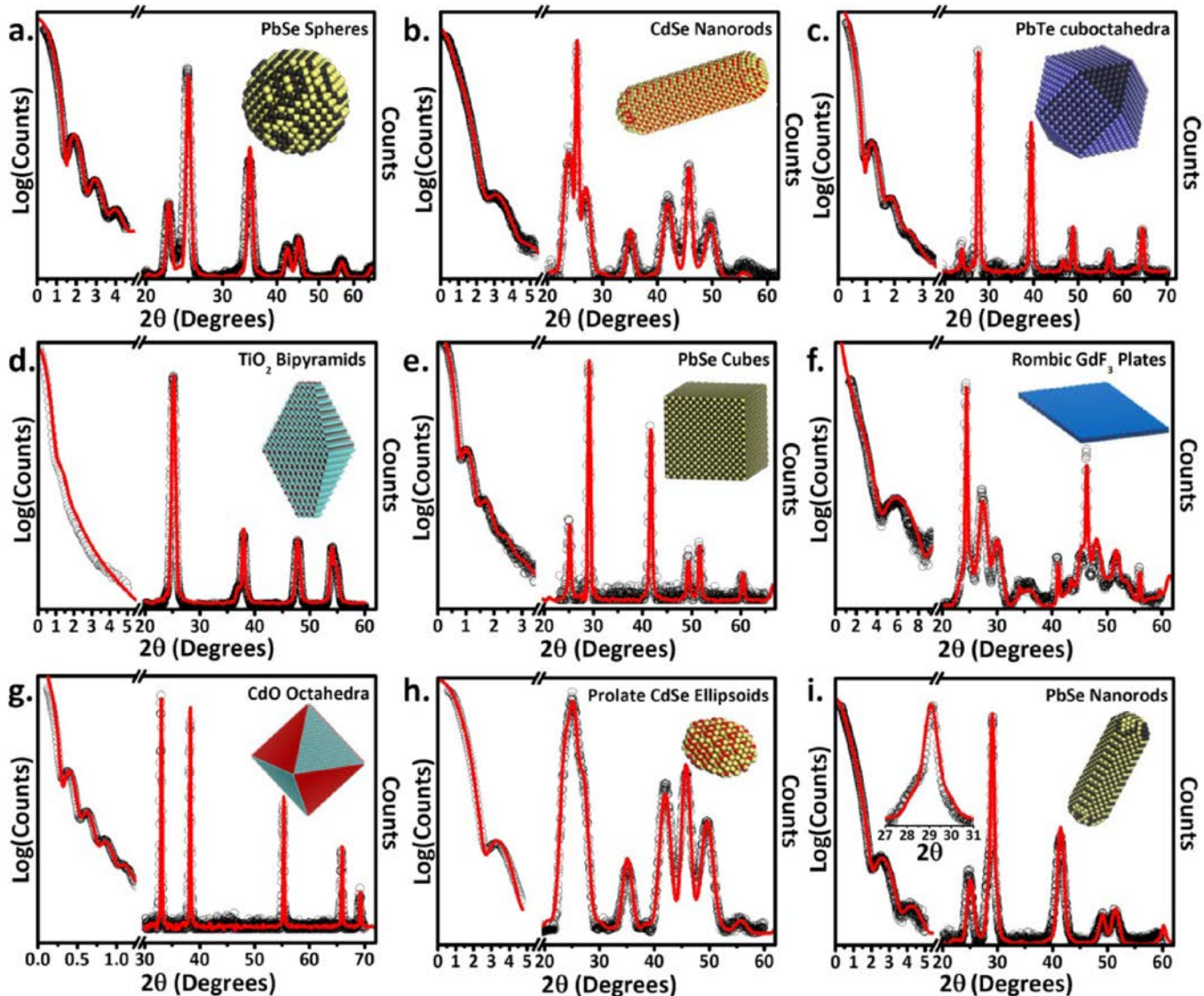


r_{mn} is the distance between atoms m and n , with atomic form factors F_m and F_n ,



The Debye approach holds for both small and wide angle scattering data, and it is applicable to crystalline, partially crystalline and amorphous samples.

Combining SAXS and WAXS

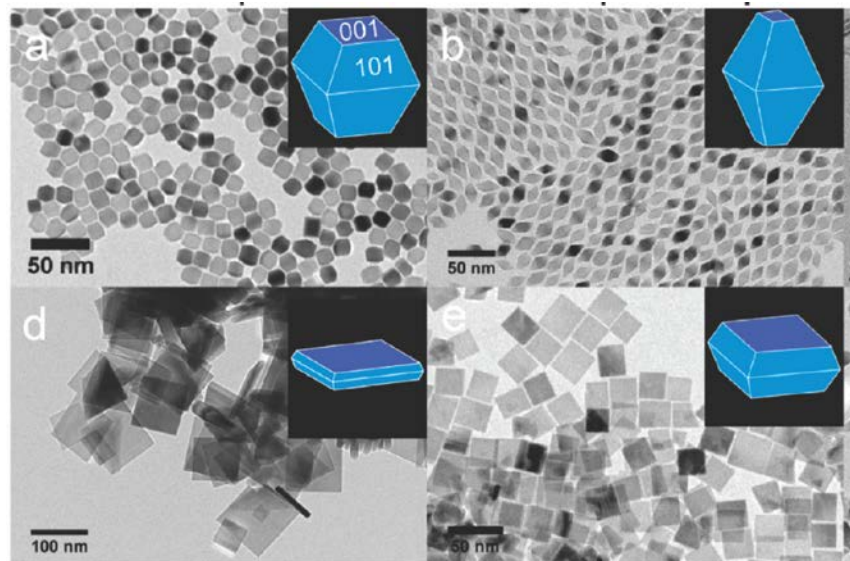


T. Gordon et al., Chem. Mater. 2015, 27, 2502–2506

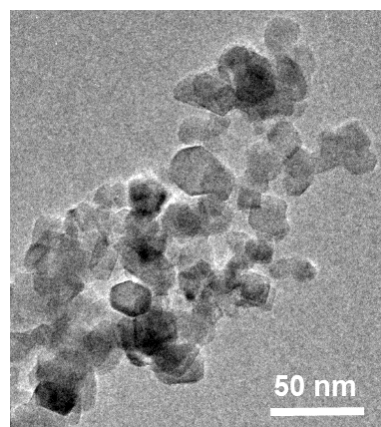
School on Synchrotron Radiation “Gilberto Vlaic”

Why X-rays and not electron microscopy?

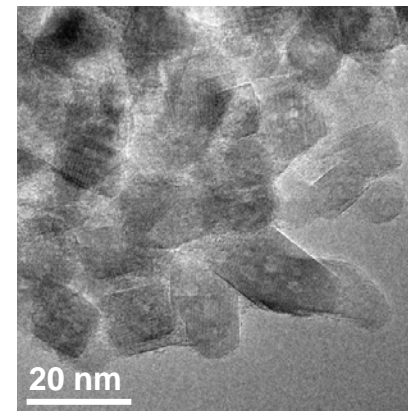
Shape-controlled NPs



Industrial commercial NPs



TiO₂ P25 (Evonik)



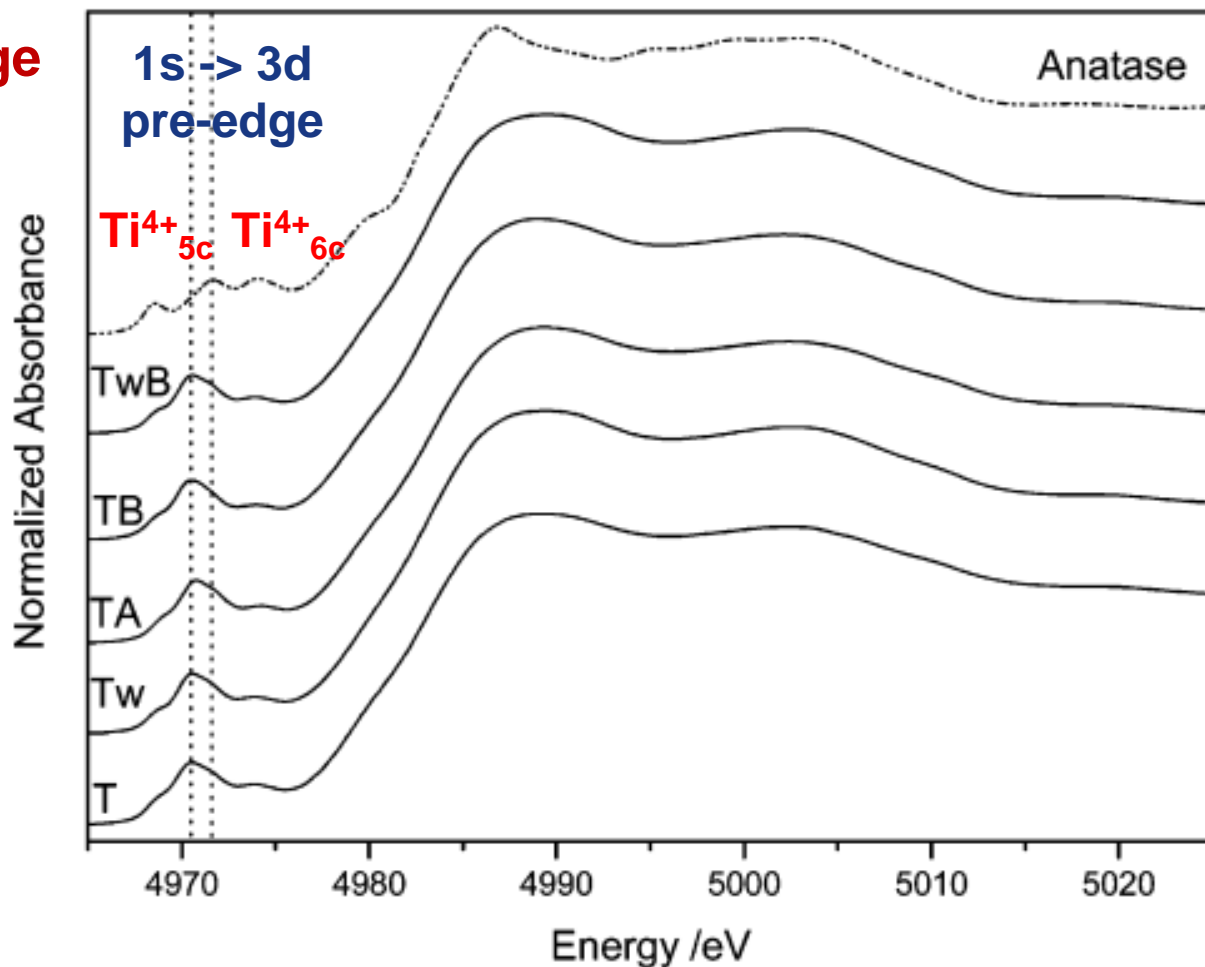
TiO₂ T-SP (Solaronix)

In «real» commercial samples the NPs heterogeneity often makes the extraction of statistically significant information from TEM images laborious and subject to bias

Combining scattering and spectroscopy

Study of the crystallization process from amorphous TiO_2 to anatase

Ti K-edge
XAS

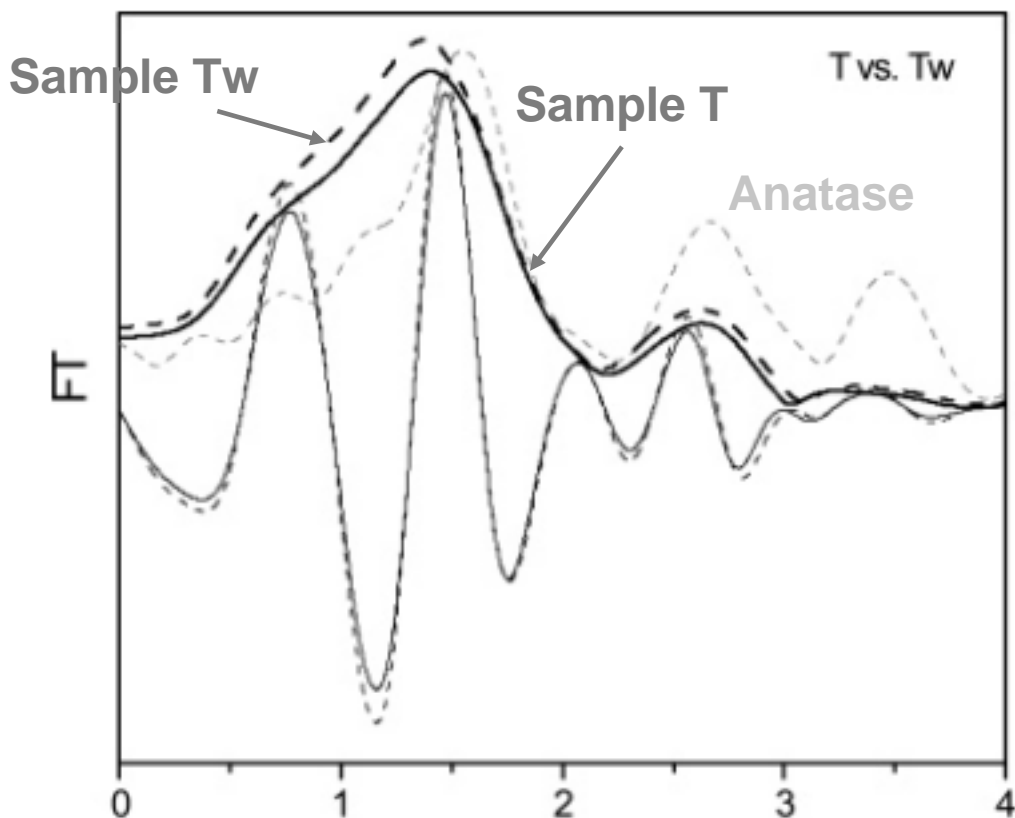


M. Fernandez-Garcia et al., J. Am. Chem. Soc. 2007, 129, 13604 - 13612

XANES highlights the presence of Ti^{4+}_{5c} in amorphous TiO_2 .

Ti K-edge EXAFS analysis

M. Fernandez-Garcia et al., J. Am. Chem. Soc. 2007, 129, 13604 - 13612

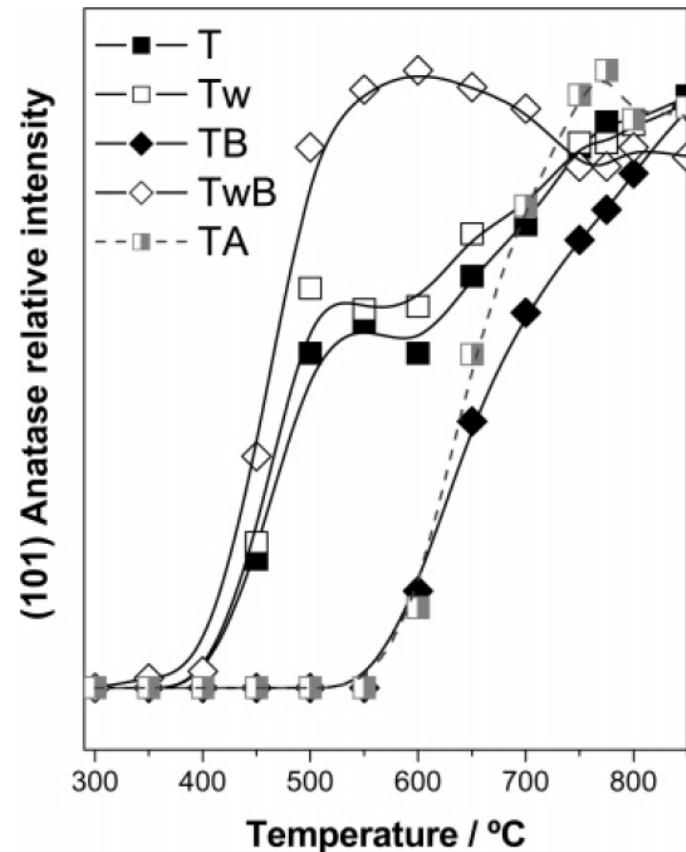
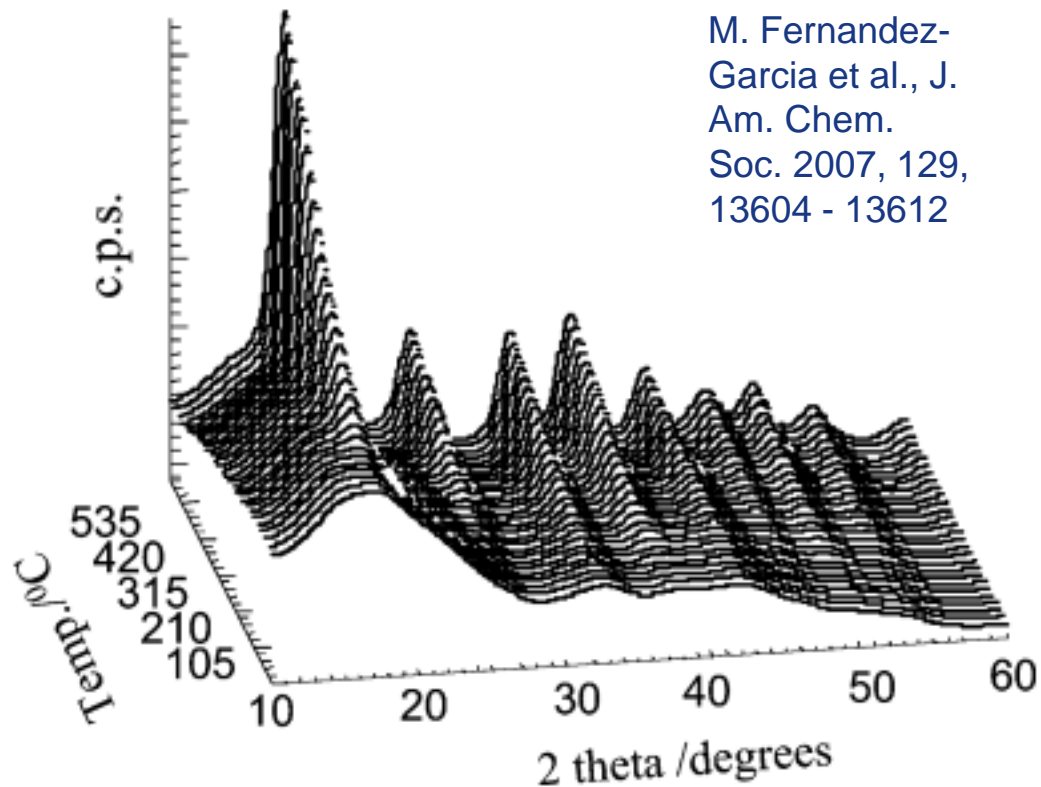


shell	N	$R/\text{\AA}$	$\Delta\sigma/10^3 \times \text{\AA}^2$
T; 7.7% ^a			
Ti-O	1.25 ± 0.35	1.72 ± 0.02	10.1 ± 0.4
Ti-O	5.1 ± 0.6	1.91 ± 0.01	7.5 ± 0.7
Ti-Ti	1.9 ± 0.3	3.02 ± 0.01	2.0 ± 0.6
Tw; 8.9%			
Ti-O	1.45 ± 0.4	1.73 ± 0.02	9.0 ± 0.5
Ti-O	5.3 ± 0.7	1.90 ± 0.01	8.5 ± 0.6
Ti-Ti	2.2 ± 0.3	3.03 ± 0.01	1.7 ± 0.6
TA, 11.1%			
Ti-O	1.25 ± 0.35	1.72 ± 0.02	9.5 ± 0.3
Ti-O	5.0 ± 0.7	1.90 ± 0.01	7.0 ± 0.7
Ti-Ti	2.3 ± 0.35	3.04 ± 0.01	1.5 ± 0.8
TB; 8.7%			
Ti-O	1.3 ± 0.3	1.72 ± 0.02	9.0 ± 0.3
Ti-O	5.1 ± 0.7	1.90 ± 0.01	7.0 ± 0.5
Ti-Ti	2.2 ± 0.3	3.02 ± 0.01	2.4 ± 0.8
TwB; 5.7%			
Ti-O	1.4 ± 0.35	1.74 ± 0.02	9.1 ± 0.4
Ti-O	5.3 ± 0.7	1.92 ± 0.01	8.0 ± 0.4
Ti-Ti	2.6 ± 0.3	3.05 ± 0.01	1.0 ± 0.9

Low Ti - Ti coordination numbers (for crystalline anatase CN = 4) suggests that Ti cations have a severely restricted 3D connectivity in all samples.

In situ XRD patterns during heating

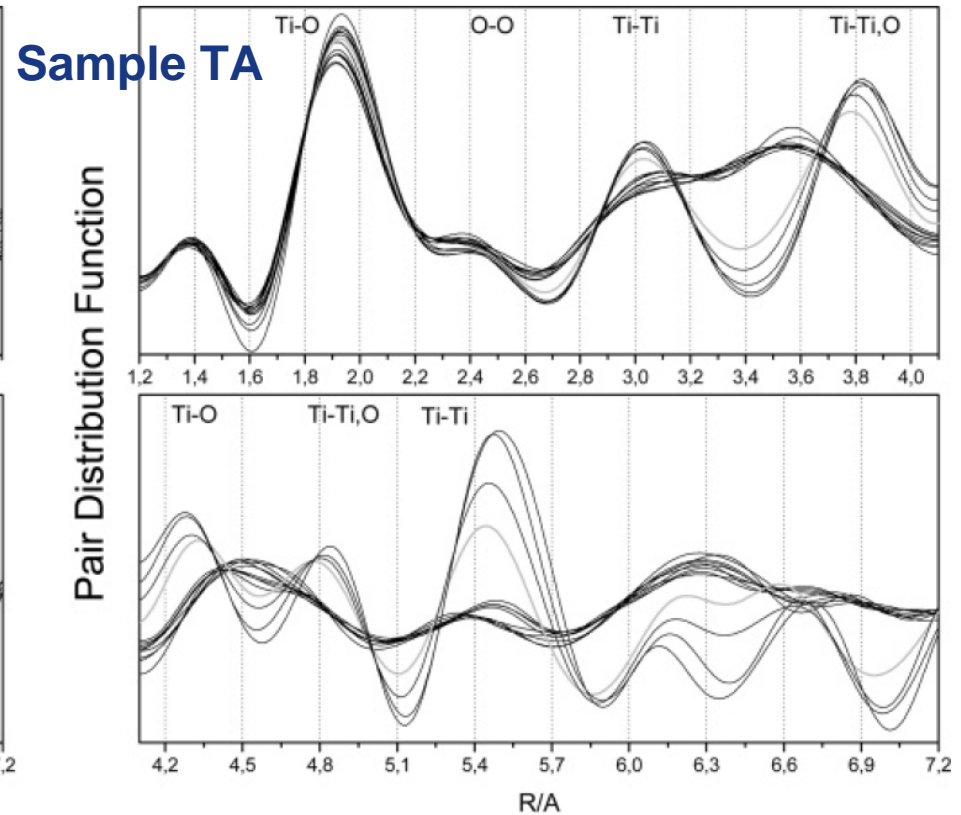
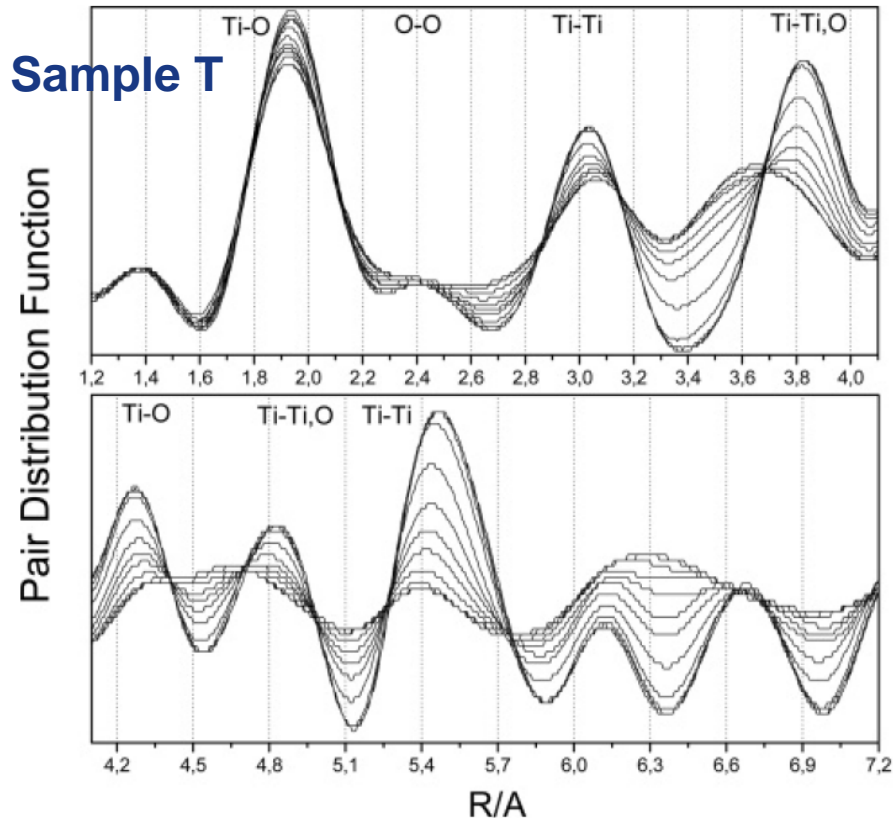
M. Fernandez-Garcia et al., J. Am. Chem. Soc. 2007, 129, 13604 - 13612



Upon heating in dry air, samples T, Tw, and TwB nucleate around 350 - 400 °C, samples TA and TB nucleate around 550 °C

Monitoring crystallization by PDF

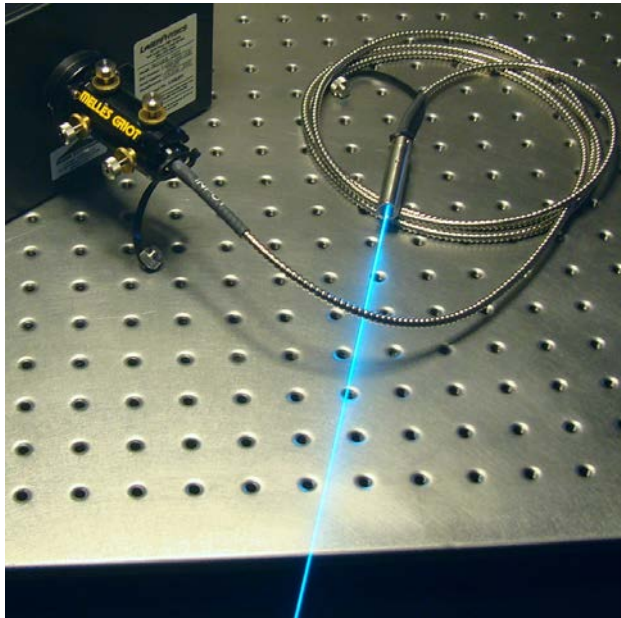
PDF obtained during heating in dry air in step of 50 °C



Crystallization onset temperature is clearly related to the local middle range order (3 - 4 Å) of the different samples

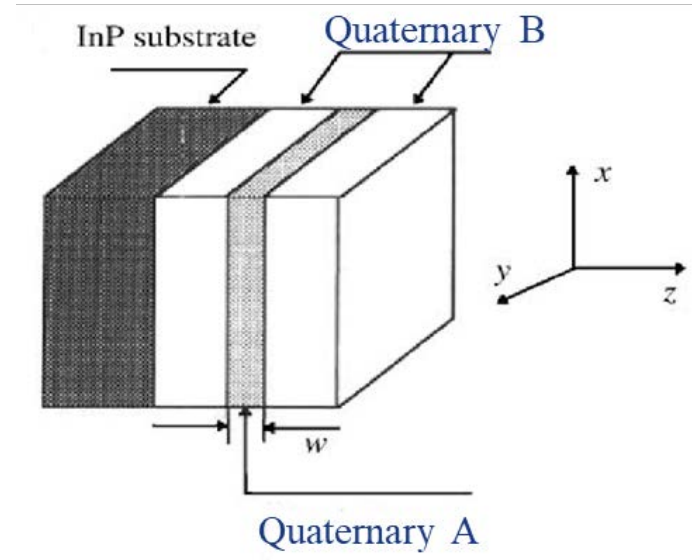
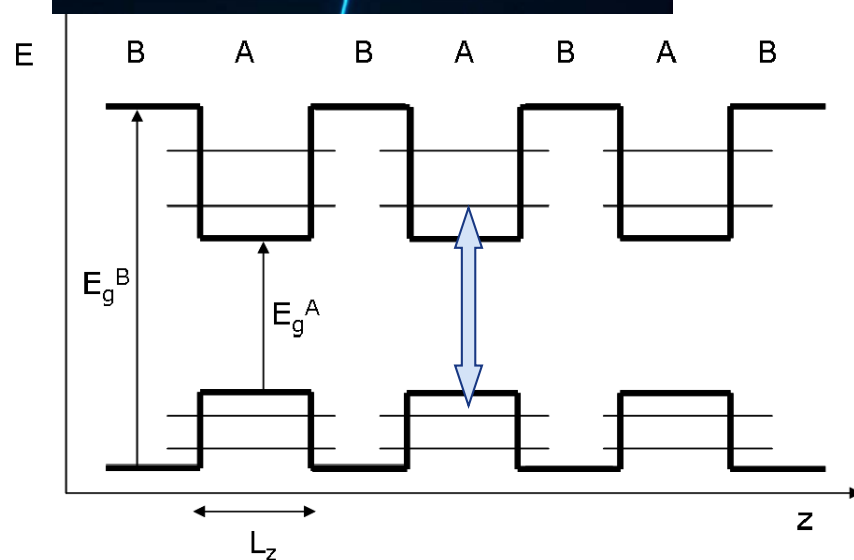
**Let's jump to a
more complex case:
real devices...**

Nanostructured device characterization



Semiconductor nanostructures to realize lasers and modulators for fiber-optics communications

Both laser and modulator are $\text{In}_x\text{Ga}_y\text{Al}_{1-x-y}\text{As}$ multi quantum well (MQW) heterostructures grown on $\text{InP}(001)$



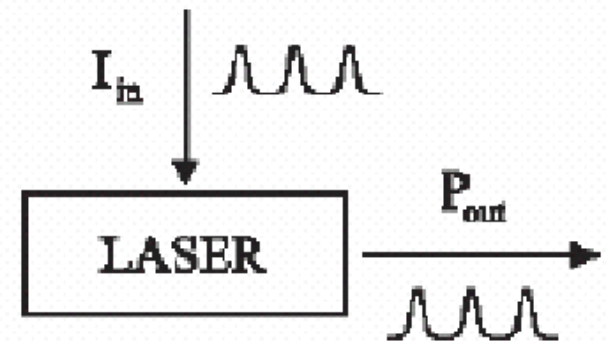
Signal modulation for fiber-optic communication

The signal can be modulated in two different ways:

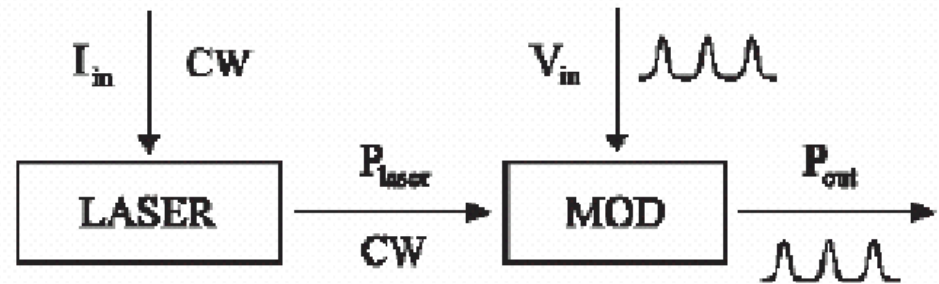
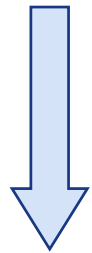
- **Direct:** modulating the laser current



non equilibrium in the charge carriers causes frequency shifts in the emitted radiation

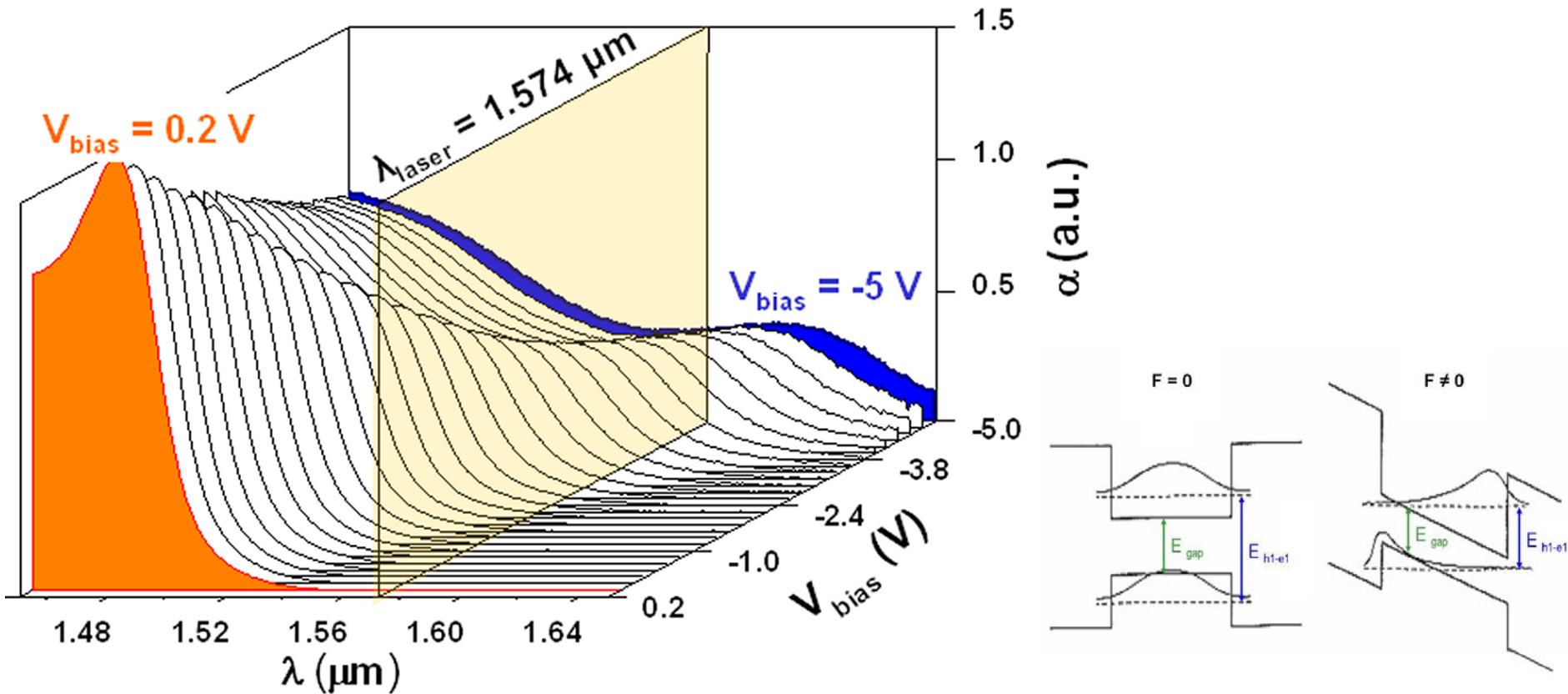


- **External:** two different devices act as laser source and signal modulator



both the frequency (Gbit/s) and transmission lengths are improved

Electro-absorption modulator (EAM)



L. Mino et al., *Small* 2011, 7, 930-938

A suitable voltage switches the EAM from transparent to opaque (Stark effect)

Modulator (EAM)- DFB laser inte

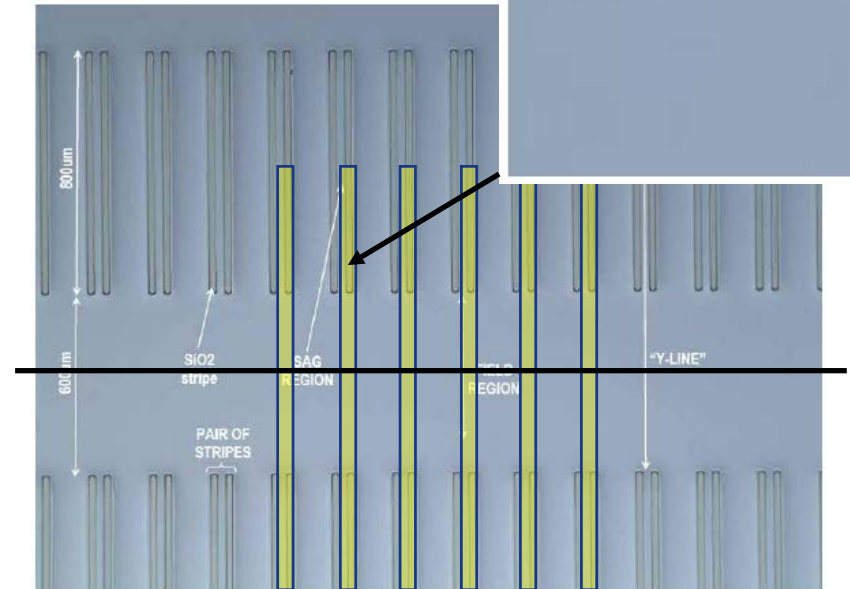
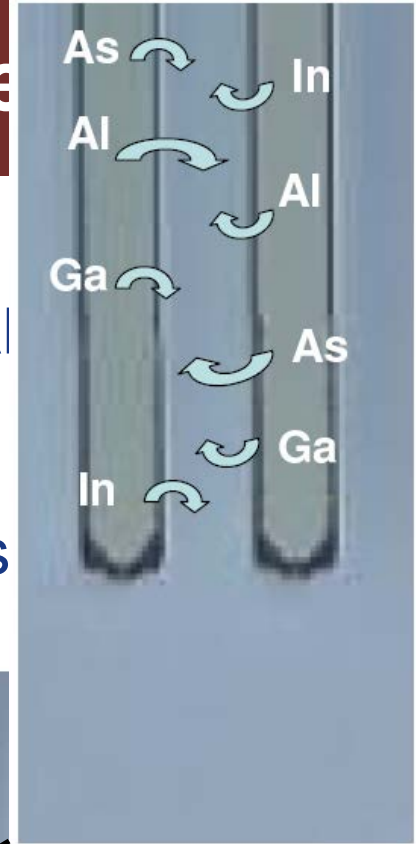
Monolithic integration of the laser and the EAM



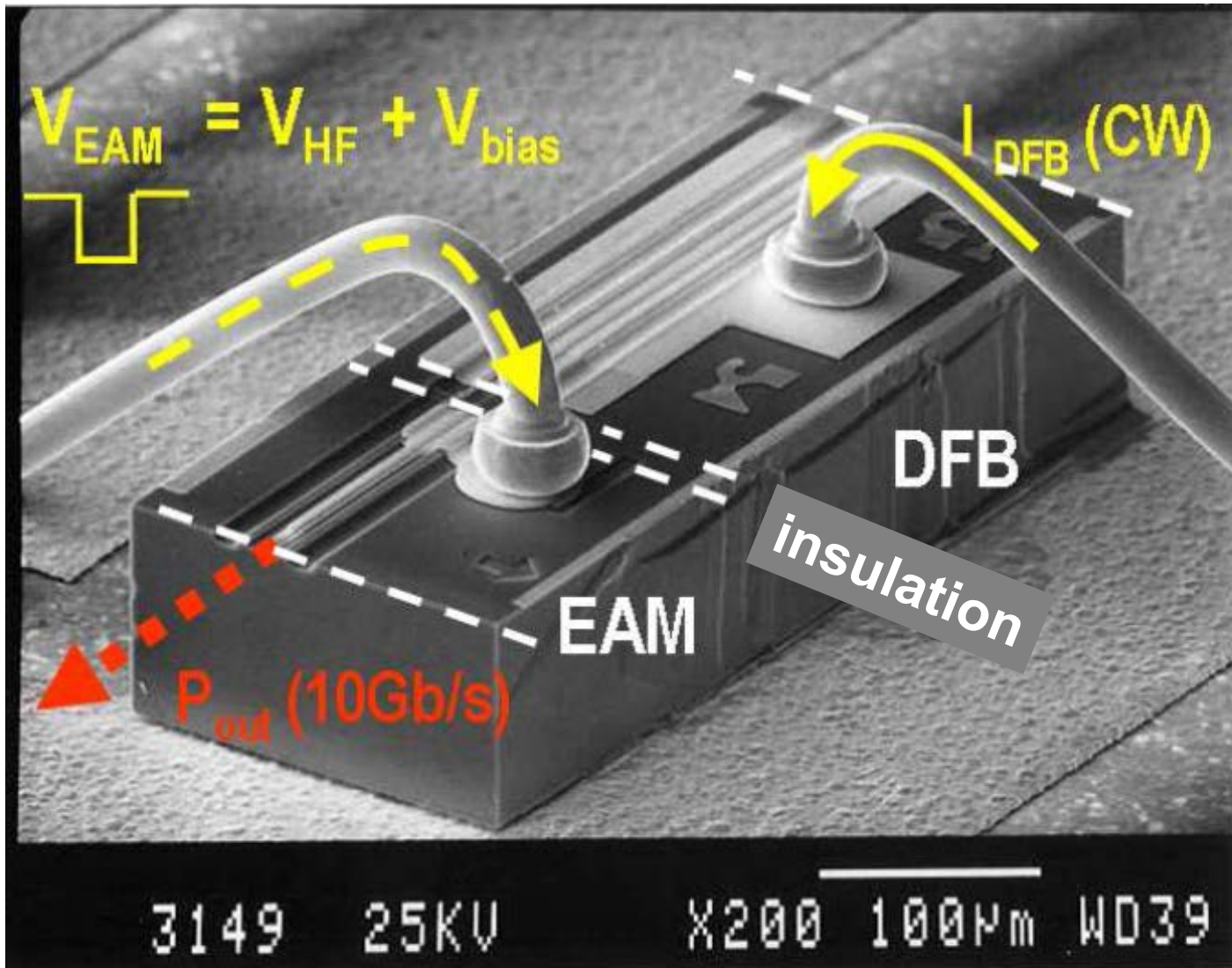
Selective Area Growth (SAG): a SiO_2 mask
the precursors flux



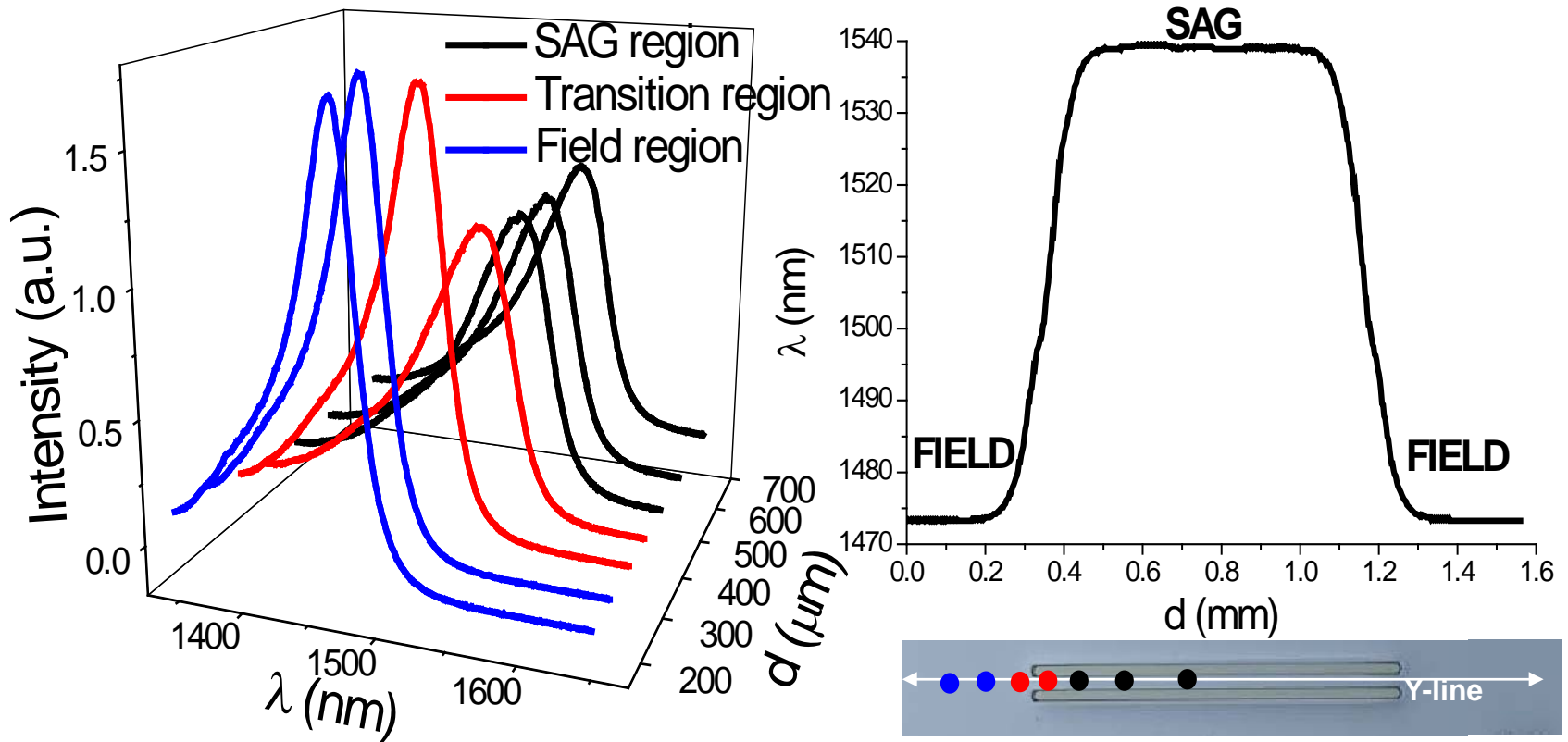
variation in composition
and thickness of the
material grown between
the SiO_2 stripes



The complete modulator-laser device



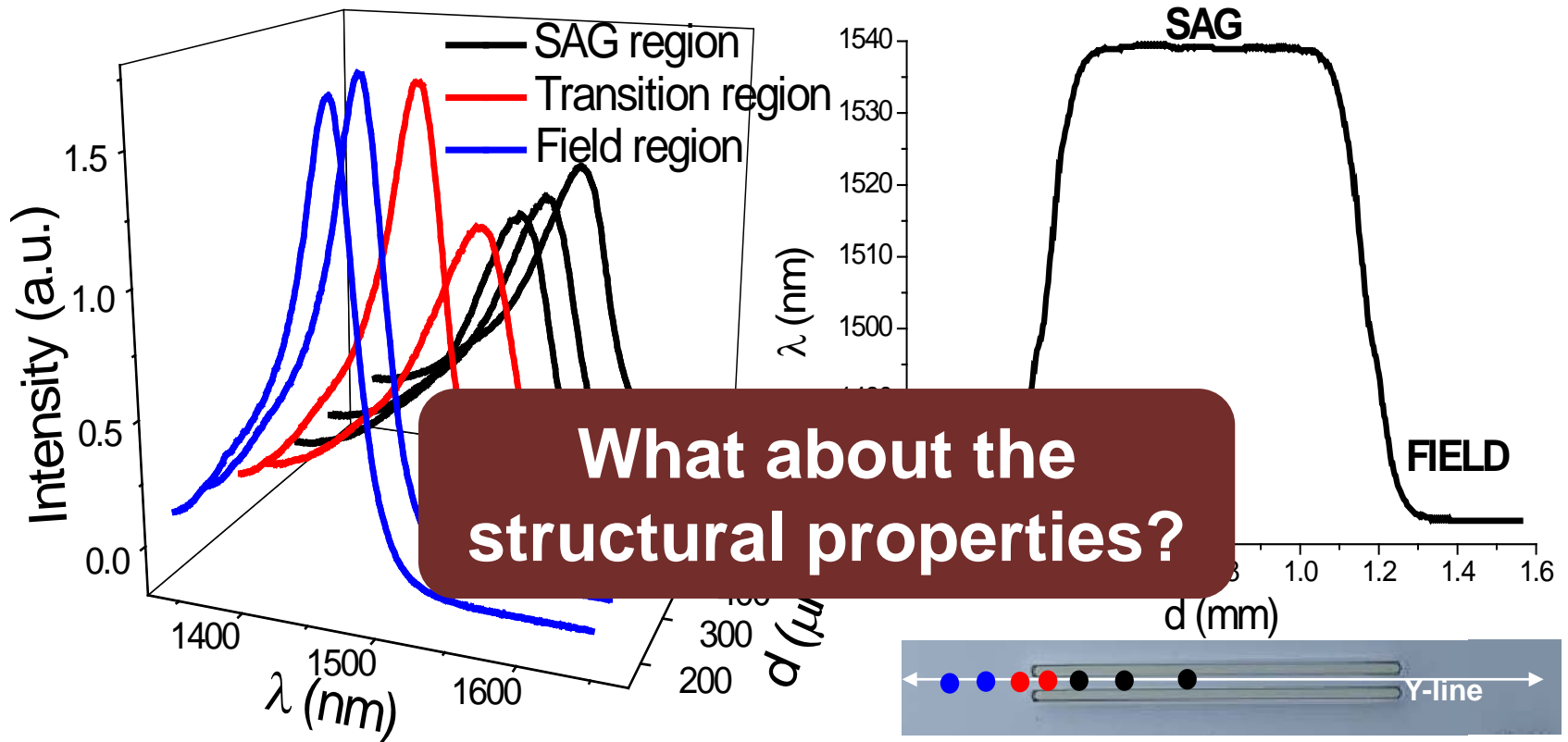
Energy gap space-resolved determination



Space resolved photoluminescence (PL) study with a $15 \mu\text{m}$ resolution along a line parallel to the SiO_2 stripes (Y-line)

L. Mino et al., Adv. Mater. 2010, 22, 2050-2054

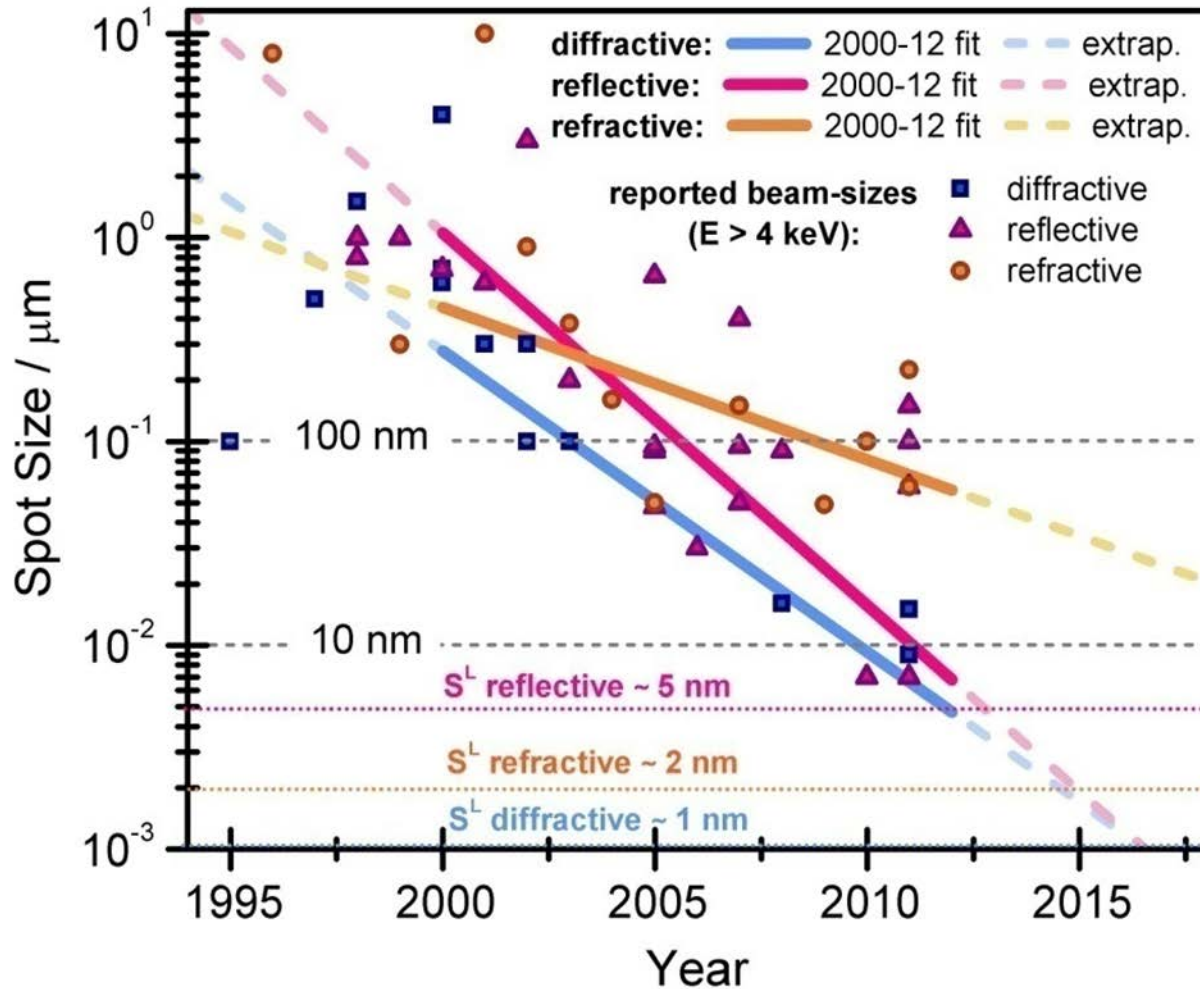
Energy gap space-resolved determination



Space resolved photoluminescence (PL) study with a 15 μm resolution along a line parallel to the SiO₂ stripes (Y-line)

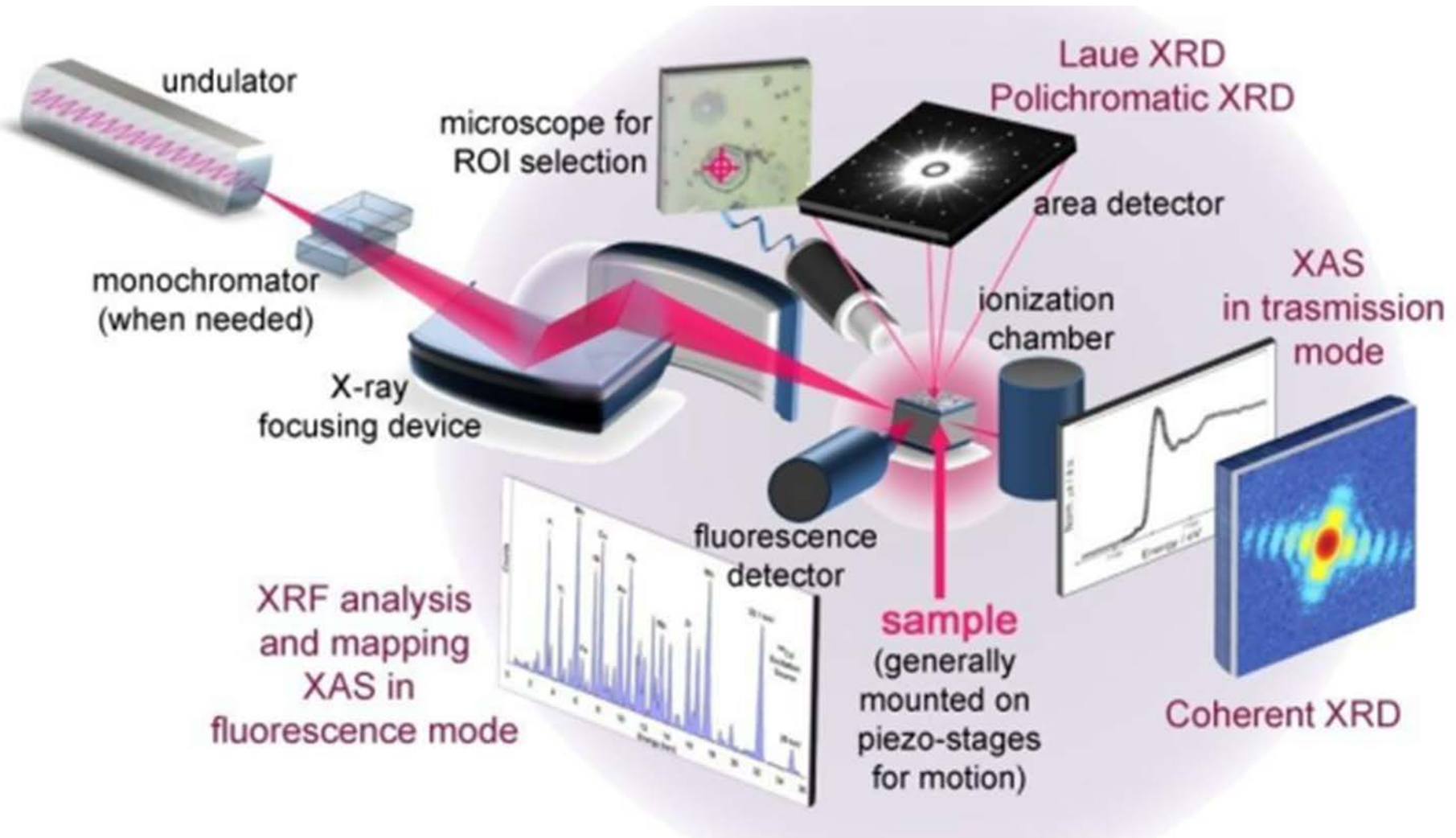
L. Mino et al., Adv. Mater. 2010, 22, 2050-2054

Synchrotron X-ray micro-/nano-beams



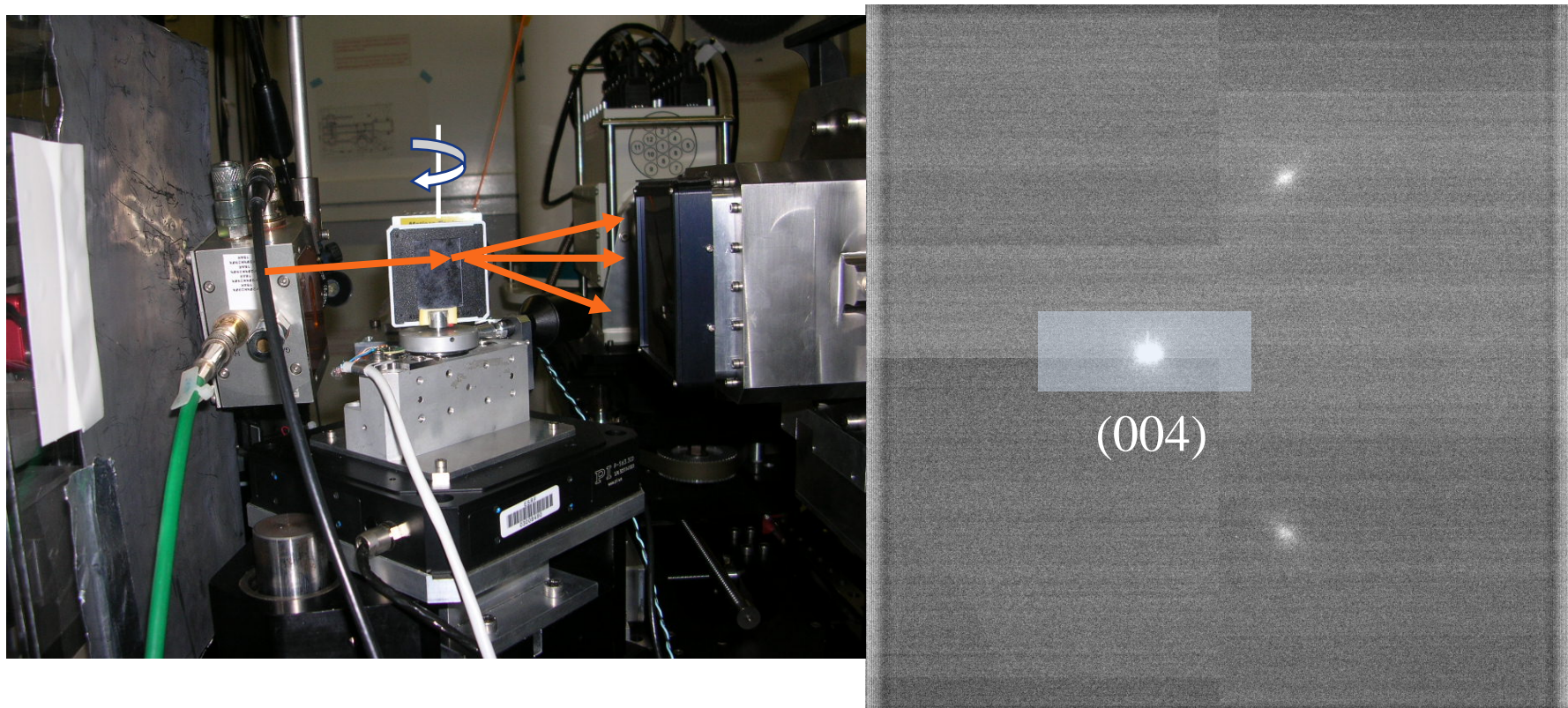
L. Mino et al., Rev. Mod. Phys. 2018, 90, 025007

ESRF ID22 beamline (now ID16)



X-ray micro-beam: $1.7 \mu\text{m} \times 5.3 \mu\text{m}$

Micro-XRD experimental setup

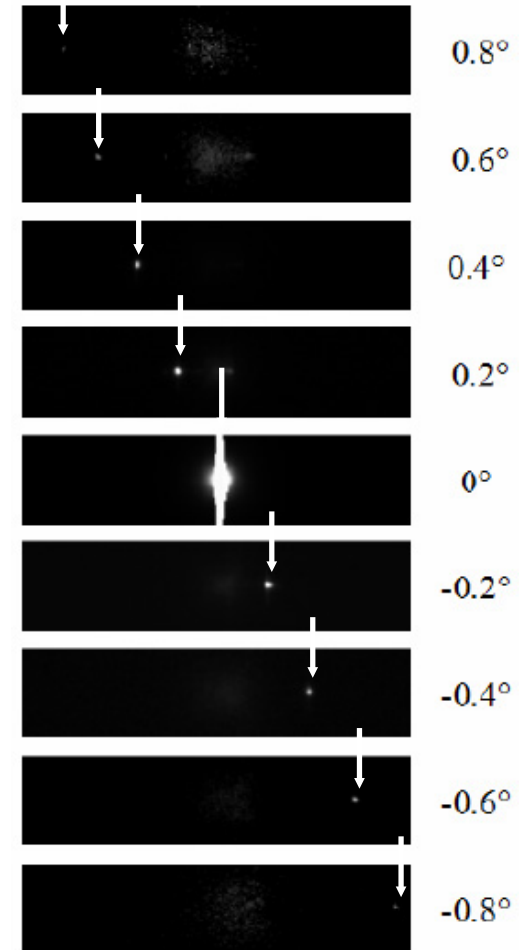
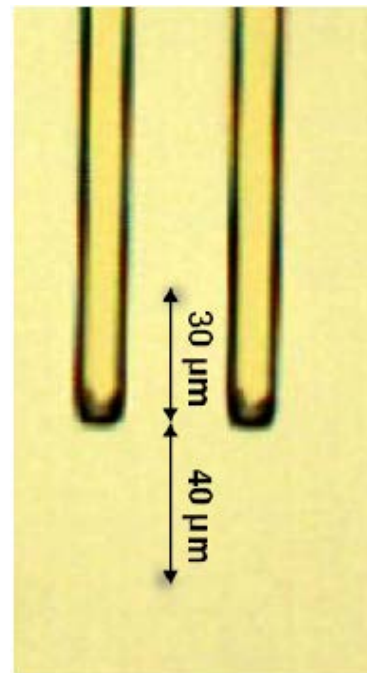


CCD image

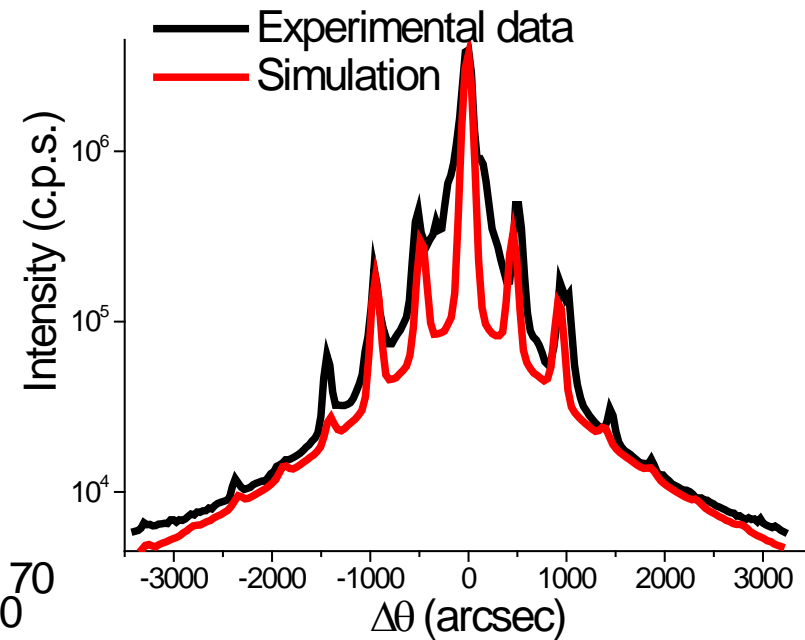
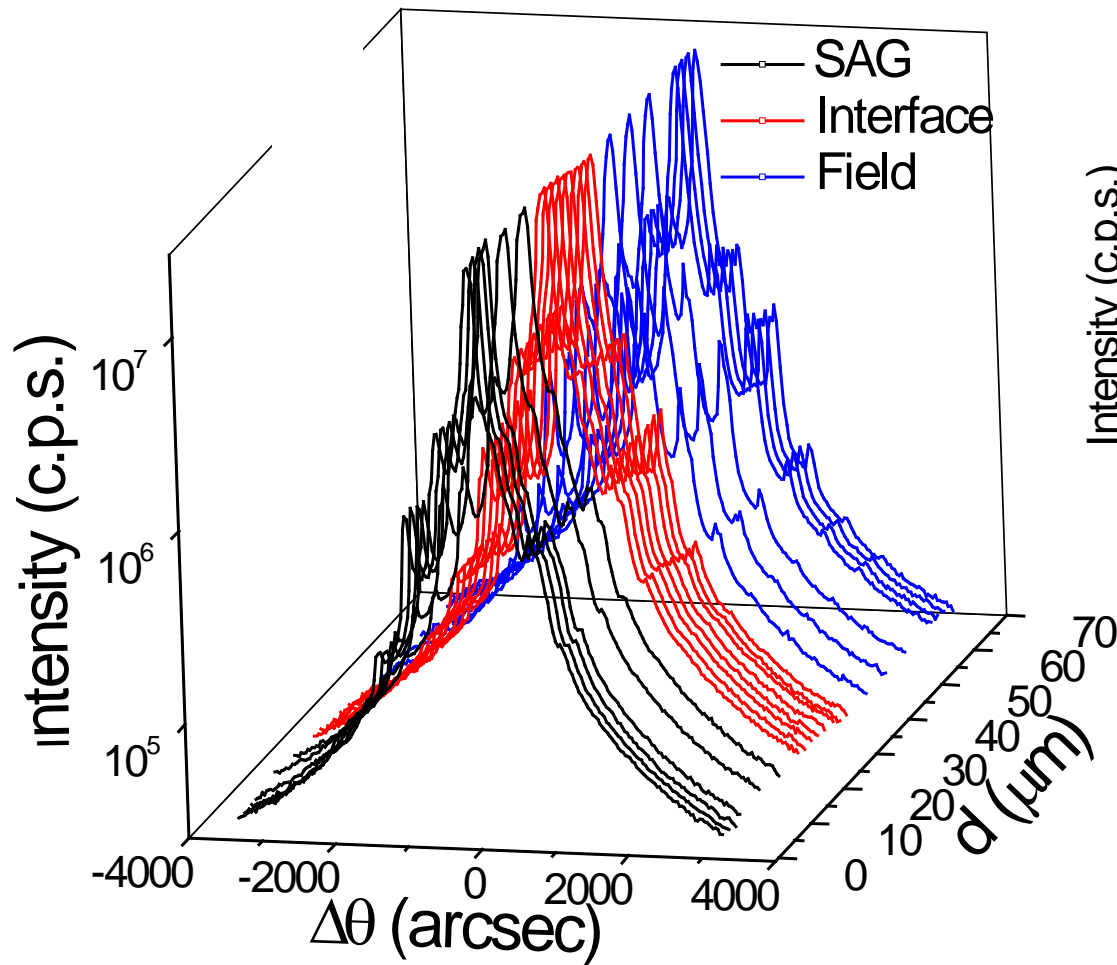
Micro-XRD pattern acquisition

176 images covering a rotation of $\pm 1.1^\circ$ around the InP(004) Bragg angle ($\theta_B = 14.359^\circ$ at 17 keV)

35 different points have been sampled along the Y-line with $2\ \mu\text{m}$ resolution



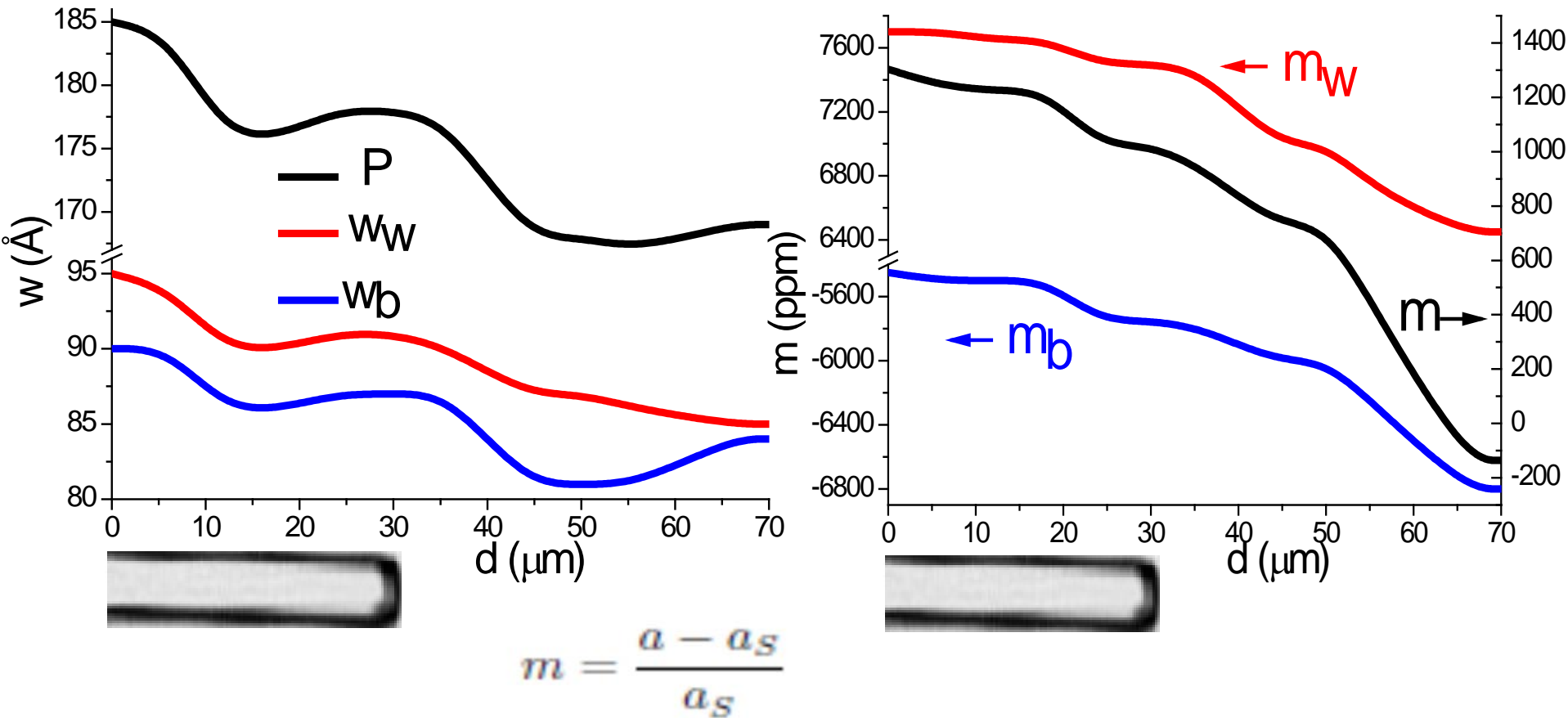
Reconstruction of the XRD patterns



Each XRD pattern
reconstructed starting from
the 176 CCD images

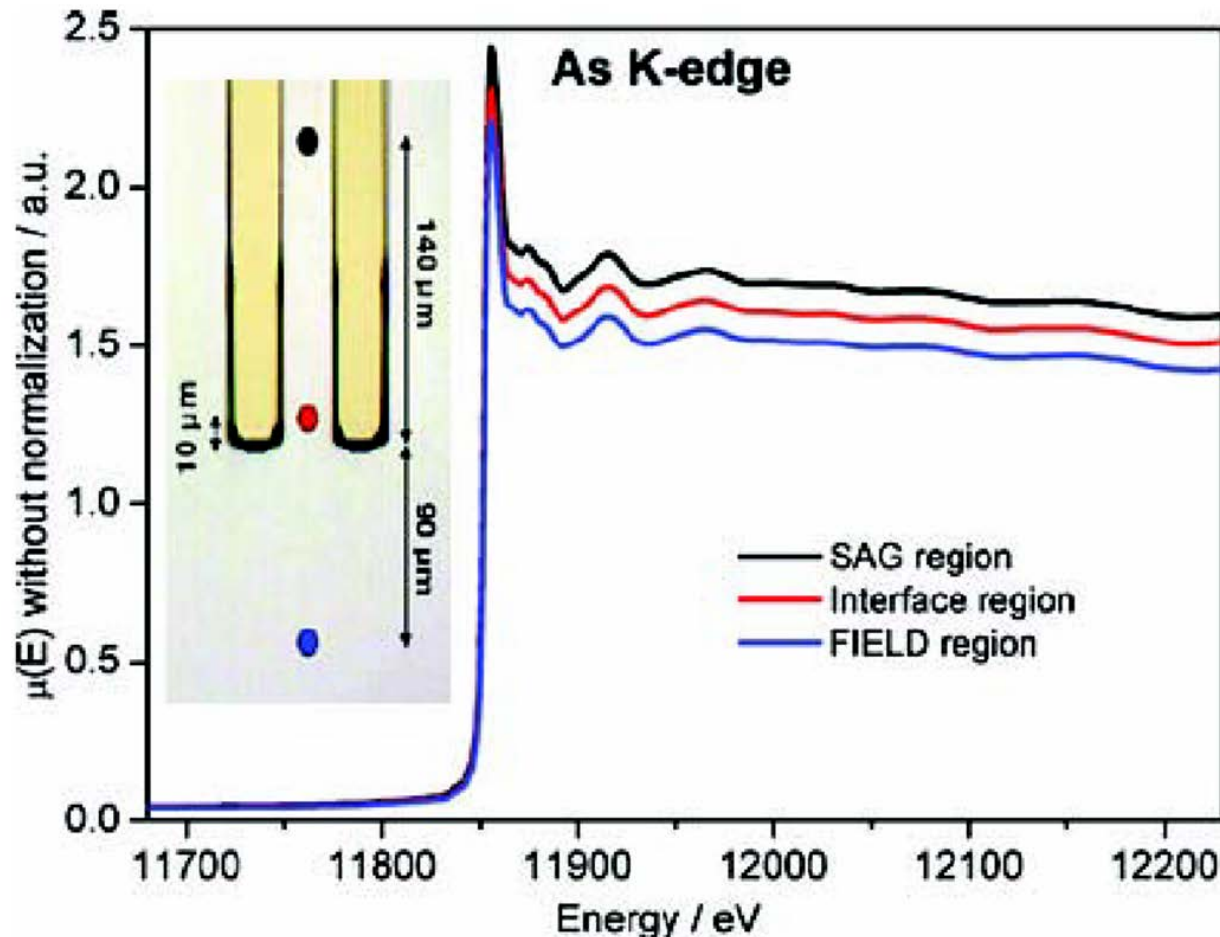
L. Mino et al., Adv. Mater. 2010, 22, 2050-2054

Space-resolved XRD results



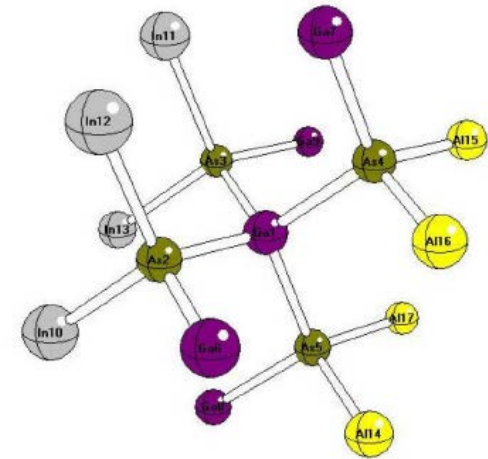
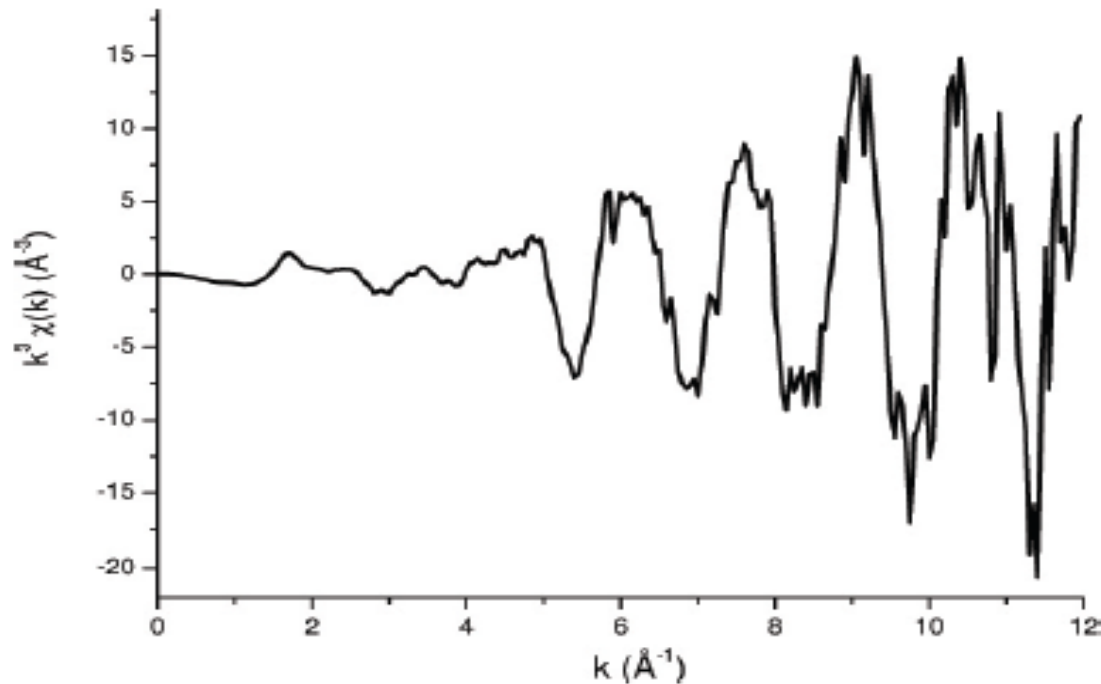
Widths (w_b , w_w) and mismatches (m_b , m_w) of the MQW barrier and of the well obtained performing a fitting of the XRD patterns

X-ray absorption spectroscopy



Local structural information on the $\text{In}_x\text{Ga}_y\text{Al}_{1-x-y}\text{As}$ semiconductor combining micro-XAS at the Ga K-edge and As K-edge

EXAFS signal extraction

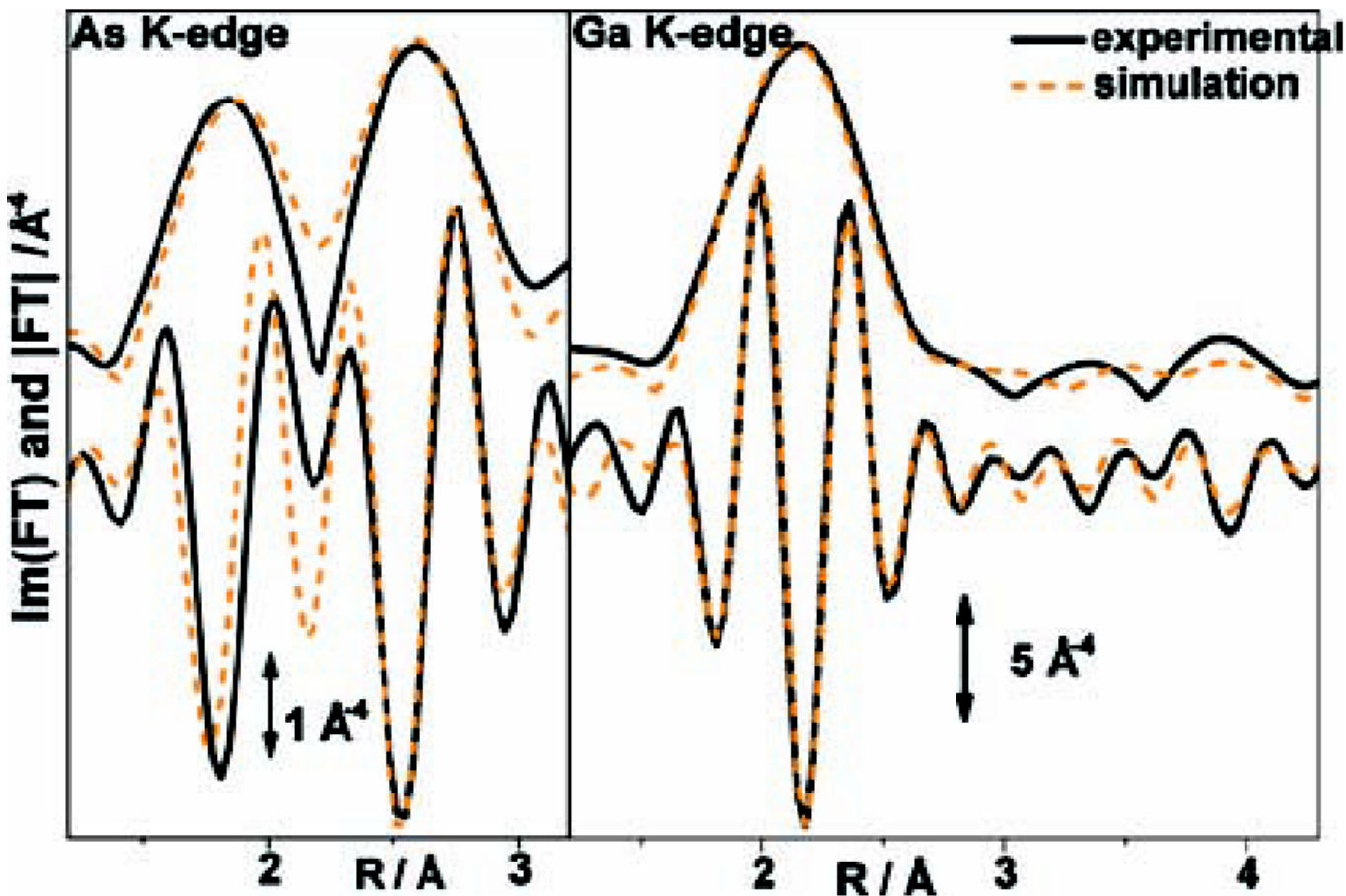


EXAFS signal:

$$\chi = \frac{\mu - \mu_0}{\mu_0}$$

$$\chi(k) = \sum_j \frac{N_j}{R_j^2} e^{-2\frac{R_j}{\lambda}} e^{-2k^2\sigma_j^2} A_j(k, \pi) \sin[2kR_j + \varphi(k, R_j, \pi)]$$

EXAFS data fitting



L. Mino et al., *Small*
2011, 7, 930-938

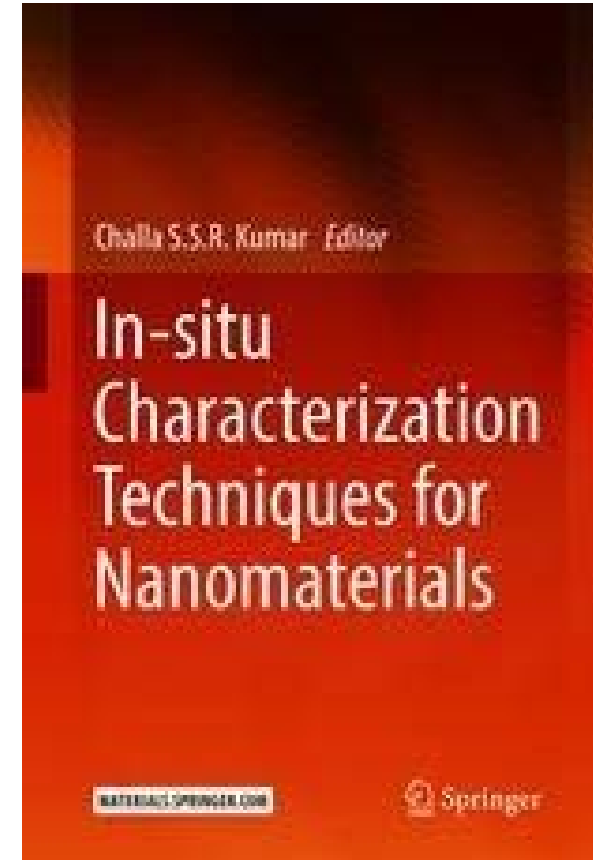
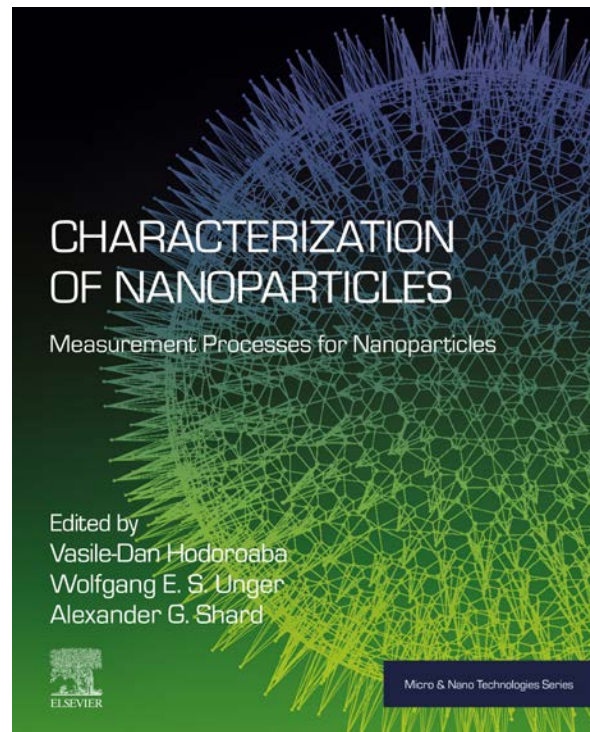
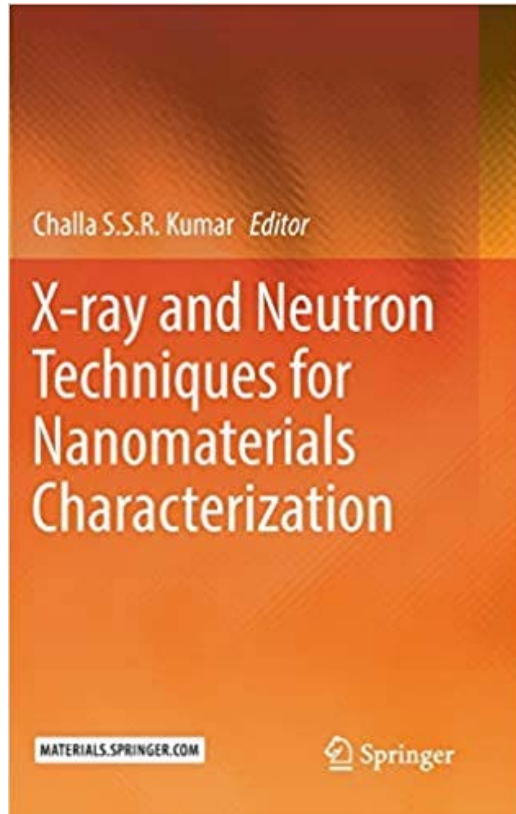
For the fit a co-refinement approach was adopted using the following intervals in k - and R -spaces: $3.0\text{--}9.0 \text{\AA}^{-1}$ and $1.0\text{--}3.2 \text{\AA}$ for As K-edges, $3.0\text{--}10.8 \text{\AA}^{-1}$ and $1.0\text{--}4.3 \text{\AA}$ for Ga K-edges

EXAFS results

Parameter	SAG	FIELD
$R_{\text{As-Ga}}$ [Å]	2.469 ± 0.007	2.463 ± 0.005
$\Delta R_{\text{As-Ga}}$ [Å]	0.021 ± 0.007	0.015 ± 0.005
$R_{\text{As-In}}$ [Å]	2.60 ± 0.02	2.60 ± 0.02
$\Delta R_{\text{As-In}}$ [Å]	-0.02 ± 0.02	-0.02 ± 0.02
$R_{\text{As-Al}}$ [Å]	2.49 ± 0.11	2.48 ± 0.11
$\sigma^2_{\text{As-Ga}}$ [Å ²]	0.006 ± 0.002	0.005 ± 0.002
$\sigma^2_{\text{As-In}}$ [Å ²]	0.008 ± 0.003	0.007 ± 0.003
$\sigma^2_{\text{As-Al}}$ [Å ²]	0.010 ± 0.004	0.008 ± 0.004

L. Mino et al., Small 2011, 7, 930-938

Further reading



Further reading

IOP PUBLISHING

J. Phys. D: Appl. Phys. **46** (2013) 423001 (72pp)

JOURNAL OF PHYSICS D: APPLIED PHYSICS

doi:10.1088/0022-3727/46/42/423001

TOPICAL REVIEW

Low-dimensional systems investigated by x-ray absorption spectroscopy: a selection of 2D, 1D and 0D cases

Lorenzo Mino¹, Giovanni Agostini¹, Elisa Borfecchia¹,
Andrea Piovano³, Erik Gallo^{1,4} and Carlo Lamberti¹



Progress in Materials Science 112 (2020) 100667

Contents lists available at [ScienceDirect](#)

Progress in Materials Science

journal homepage: www.elsevier.com/locate/pmatsci

Watching nanomaterials with X-ray eyes: Probing different length scales by combining scattering with spectroscopy

Cinzia Giannini^a, Vaclav Holy^{b,c}, Liberato De Caro^a, Lorenzo Mino^d, Carlo Lamberti^{e,f}

Materials characterization by synchrotron x-ray microprobes and nanoprobe

Lorenzo Mino, Elisa Borfecchia, Jaime Segura-Ruiz, Cinzia Giannini, Gema Martinez-Criado, and Carlo Lamberti

Rev. Mod. Phys. **90**, 025007 – Published 28 June 2018

An aerial photograph of the Colorado State Capitol building in Denver, Colorado, taken at dusk. The building's iconic dome is illuminated from below, and the surrounding city lights are visible against the twilight sky. The Rocky Mountains are seen in the distance under a soft, colorful sky.

**Thank you for
your attention!**